

Response to Interactive comment on “Modeling photosynthesis of discontinuous plant canopies by linking Geometric Optical Radiative Transfer model with biochemical process” by Q. Xin et al.

We thank the reviewer for the constructive comments. We studied the comments and revised the draft accordingly. Our responses to the comments follow below.

General comments: This ms provided a useful study to model GPP of discontinuous plant canopies using GORT model. The analytical solutions are good and quite informative. The most interesting thing I think is that authors tries to separate the canopy into sunlit and shaded parts and integrated into GORT models. This is evidently an advance to current research and would be quite useful for future GPP modeling. I think the ms needs some moderate revision before final publication.

1. It is not clear that why authors selected two deciduous sites. The reason I have is that GPP of deciduous sites are much “easier” to simulate than evergreen forests. Also, the GORT for evergreen sites might be quite different from deciduous ones. Second, even for these two sites, there are more data available in the flux database. Why only part of them was used? For example, for Harvard site, the data could be from 1994 - 2010. If the analytical solutions are the same, then I would guess the validation should be easy to implement.

Reply: thank you for your advice. One reason that we chose to validate our model with two deciduous sites is that one of us (Q.X.) conducted fieldworks on both forest sites in the summer of 2009. In the fieldwork, we measured tree parameters and performed ground-based Lidar scans. We considered that tree crowns in both sites could be approximated by ellipsoidal shapes appropriately. It is true that the current model may have difficulties to model GPP for evergreen forest stands. Tree crown shapes in boreal areas are mostly conical rather than ellipsoidal. Needle clumping within shoot clumping may also need to be considered. We would like to further develop and validate models when data from evergreen sites become available. To address your concerns, we revised our manuscript, and it reads as “Fourth, we use ellipsoids to describe tree crown shapes for deciduous broadleaf forests. Because many evergreen needleleaf forests have conical crowns, future applications to areas with conifer forests may require different treatment on crown shapes in the models.”

There are indeed more data available for these sites. For the Bartlett site, Level 4 data are available from 2004 to 2006 and Level 2 data are available from 2004 to 2011. However, GPP estimates are missed in Level 2 products; we therefore only performed analysis using Level 4 data for the years from 2004 to 2006. For the Harvard site, Level 4 data are available from 1992 to 2006 and Level 2 data are available from 1991 to 2011. To model GPP on a yearly basis, we also have to know leaf area index (LAI) as obtained from MODIS data. Based on your suggestions, we now performed model simulations for the Harvard Forest site from 2001 to 2011, and summarized the results in a table. These results now read as follows:

Table 4 lists major statistical results for our model performance, as evaluated using all available hourly data at both sites. The model performance is consistent through time and is comparable to the simulation of 8-day data (Figure 7), despite the fact that satellite-derived LAI instead of field measurements were used for yearly simulation.

Table 4. The model performance at two study sites as evaluated using hourly data. Units for root mean square error (RMSE) and mean bias error (Bias) are in $\mu\text{mol CO}_2 \text{ m}^{-2} \text{ s}^{-1}$.

Year	US-Bar			US-Ha1		
	R ²	RMSE	Bias	R ²	RMSE	Bias
2001				0.804	5.44	2.00
2002				0.729	6.75	3.09
2003				0.781	5.62	2.85
2004	0.784	4.28	1.01	0.737	6.39	1.85
2005	0.795	4.11	0.47	0.736	6.83	1.18
2006	0.801	4.31	1.06	0.777	6.49	2.28
2007				0.768	6.21	2.50
2008				0.689	7.34	3.10
2009				0.662	7.62	3.68
2010				0.752	6.55	0.35
2011				0.715	6.96	1.34

2. The GORT model is suggested to be more accurate than empirical models in GPP simulation. Also, separating the whole canopy into sunlit and shaded parts is to improve the underestimation of GPP at upper ends. In figure 11, we still see clearly that the underestimation is not solved. I think authors may give some discussion on this issue.

Reply: thank you for your insights. Separating the whole canopy into sunlit and shaded parts is to improve the biased GPP estimates. It is worth noting that sunlit leaves receive full illumination while shaded leaves only receive scattered illumination. Because there are light saturation on leaf photosynthesis, we consider the biases, if uncorrected, should be overestimates rather than underestimates at upper ends, as compared to measured GPP values. In our study, we have corrected this effect well, but it seems that there are some over-corrections. One possible reason is that we only employed empirical functions here for the correction. To understand the details, further tests on the photosynthesis – conductance model should be implemented. Another possible reason is that we only used Muneer’s method to estimate diffuse radiation components for the US-Ha1 site, which were missing in flux tower measurements. Note that there were no apparent biases for the US-Bar site in our simulations.

To address your concerns, we revised related sentences in our draft and now it reads, “There were slight GPP underestimates when measured GPP values are high at the US-Ha1 site, possibly due to empirical functions that we used in modeling diffuse radiation and leaf photosynthesis.”

3. Figure 10 showing the daily GPP simulation, and I like to see how it works at hourly time scale as shown for Harvard site.

Reply: we added a subplot in Figure 11 that shows hourly GPP simulation for the Bartlett site, and modified the related texts. It reads as follows,

For the US-Bar site, the R^2 value is 0.801 and the RMSE value is $4.31 \mu\text{mol CO}_2 \text{ m}^{-2} \text{ s}^{-1}$. For the US-Ha1 site, the correlation between modeled and measured GPP is strong with an R^2 value of 0.777 and an RMSE value of $6.49 \mu\text{mol CO}_2 \text{ m}^{-2} \text{ s}^{-1}$.

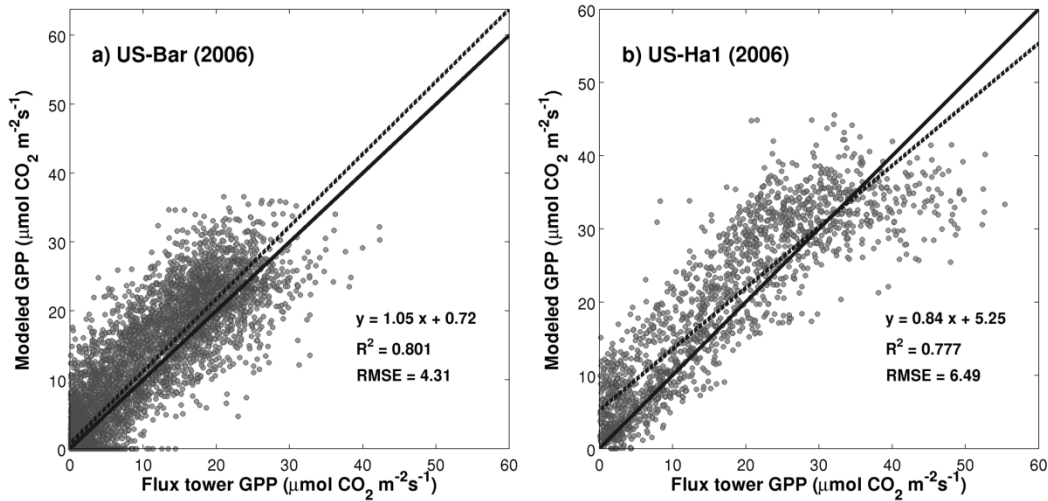


Figure 11: Regressions between modeled and measured GPP for all available hourly data at the sites of a) US-Bar and b) US-Ha1 in 2006. Only data from the photosynthetically active period are included in the regression. The solid line denotes the 1 : 1 line, and the dashed line denotes the regression line.

Thank you again for your help!

Response to Interactive comment on “Modeling photosynthesis of discontinuous plant canopies by linking Geometric Optical Radiative Transfer model with biochemical process” by Q. Xin et al.

We thank the reviewer for the constructive comments. We studied the comments and revised the draft accordingly. Our responses to the comments follow below.

This revised manuscript has incorporated most of the comments previously issued by the reviewer, and properly addressed reviewer’s questions. Now it is easier to follow, so I suggest it to be published with following minor revisions.

1. This manuscript has been based on some previous work of the community, e.g., some coefficients, so I suggest to have a table to contain the values of the coefficients, as VPD_min in current Page 3691 Line 4, and their sources.

Reply: thank you for your kind suggestion. We added another table in the appendix to describe used coefficients and their values. Now it reads as follows,

Table A2. Values for model parameters.

Symbols	Value	Units	Reference
k_C	500	W / m ²	Ding et al. (2014)
k_Q	150	W / m ²	Ding et al. (2014)
T_{min}	0	°C	Kalfas et al. (2011)
T_{max}	45	°C	Kalfas et al. (2011)
T_{opt}	25	°C	Kalfas et al. (2011)
VPD_{min}	0.65	kPa	Heinsch et al. (2003)
VPD_{max}	4.6	kPa	Heinsch et al. (2003)
VPD_0	30	kPa	Katul et al. (2000)
Γ	40	μmol/mol	Katul et al. (2000)
m_L	4.0		Katul et al. (2000)

2. What is the solar zenith angle for Figure 3b?

Reply: we now included a definition for solar zenith angle in the texts, and it reads “Extraterrestrial solar radiation and solar zenith angle (i.e., the angle that the sun away from directly overhead) are calculated ...”

3. Suggest to add two scatter plots in Figure 4 to emphasize the correspondence between measured radiation and modeled radiation.

Reply: we revised Figure 4 and the related captions. Now it reads as follows,

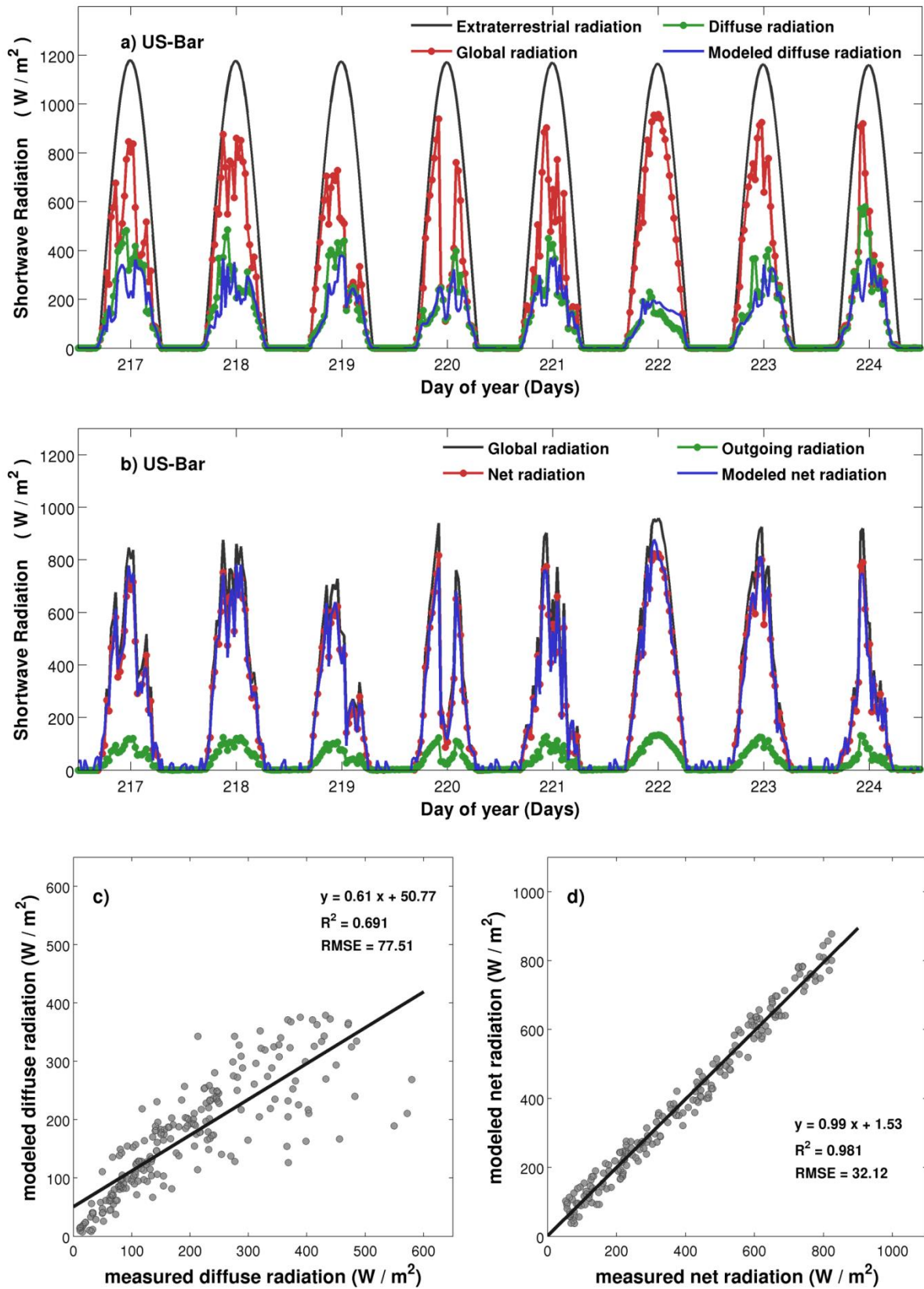


Figure 4: Measured and modeled components of radiation in 8 successive days are shown for a) the partition of global solar radiation, b) surface radiation balance, c) modeled and measured diffuse radiation, and d) modeled and measured net radiation. Extraterrestrial radiation is derived following methods outlined in Allen et al. (1998). Muneer’s method is applied to model diffuse radiation. The GORT model is applied to model net radiation. Data are shown from the Day of Year 217 to 224 in 2004 for the US-Bar site.

4. Figure caption and text relating to Figure 13 is very hard to follow, consider revising.

Reply: we revised figure captions and texts related to Figure 13 as follows,

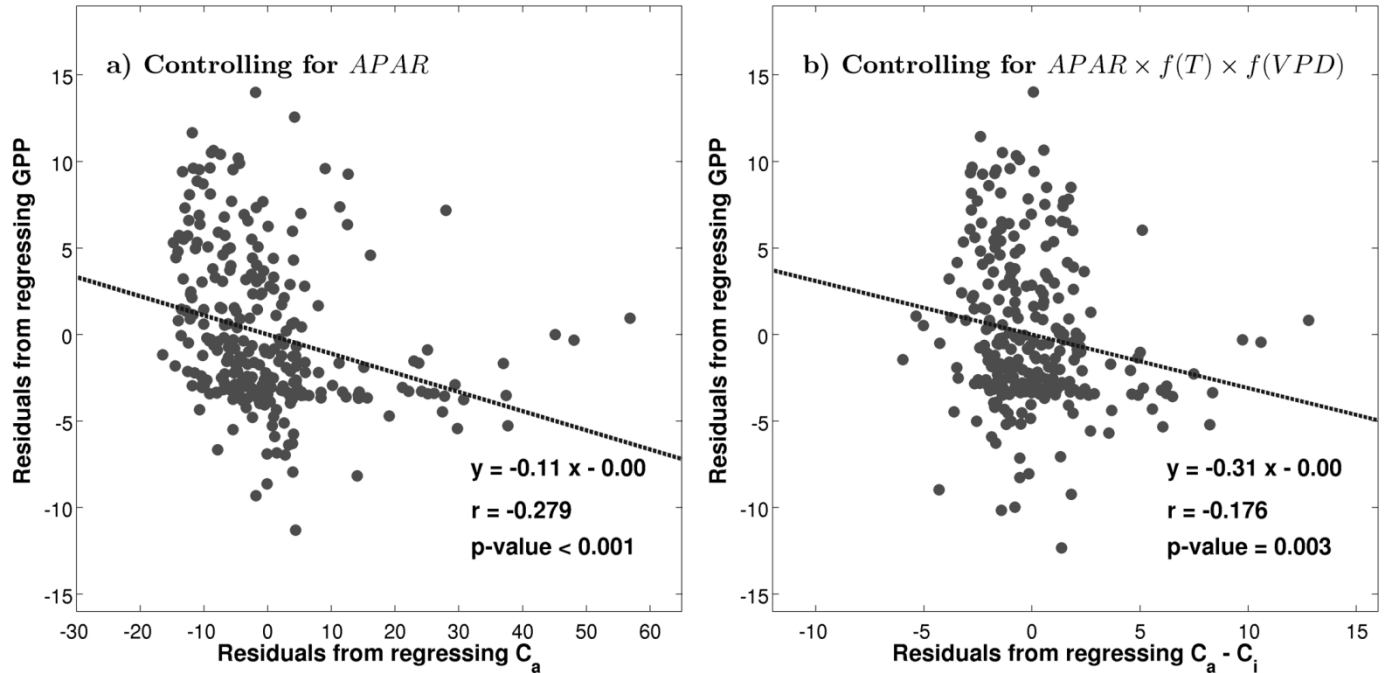


Figure 13: Residual plots are shown for a) the partial correction between GPP and ambient CO₂ concentration (C_a) while controlling for the variable of $APAR$ and b) the partial correction between GPP and $C_a - C_i$ while controlling for the variable of $APAR \times f(T) \times f(VPD)$.

5. The assertion of the last sentence in Section 5.2 has potential conflict with the statement in Ni-Meister et al., 2001, which mentioned that not accounting for the clumping and discontinuous plant canopies will lead to underestimation of biomass. Suggest to revise or delete.

Reply: thank you for your insights. We deleted relevant sentences to avoid possible conflicts.

1 **Modeling photosynthesis of discontinuous plant canopies by linking** 2 **Geometric Optical Radiative Transfer model with biochemical processes**

3 Qinchuan Xin^{1*}, Peng Gong^{1,2,3,*}, Wenyu Li¹
4

5 [1] Ministry of Education Key Laboratory for Earth System Modeling, Tsinghua University, Beijing, China

6 [2] Joint Center for Global Change Studies, Beijing, China

7 [3] Environmental Science, Policy and Management and Geography, University of California, Berkeley, CA,
8 USA

9
10 * Correspondence to: xqcchina@gmail.com (Qinchuan Xin)

11 penggong@tsinghua.edu.cn (Peng Gong)

12
13 Mailing Address:

14 Tsinghua University

15 Mengminwei South Building Room 920

16 Beijing 100084, China

17

18

Abstract

19 Modeling vegetation photosynthesis is essential for understanding carbon exchanges between terrestrial
20 ecosystems and the atmosphere. The radiative transfer process within plant canopies is one of the key
21 drivers that regulate canopy photosynthesis. Most vegetation cover consists of discrete plant crowns, of
22 which the physical observation departs from the underlying assumption of a homogenous and uniform
23 medium in classic radiative transfer theory. Here we advance the Geometric Optical Radiative Transfer
24 (GORT) model to simulate photosynthesis activities for discontinuous plant canopies. We separate radiation
25 absorption into two components that are absorbed by sunlit and shaded leaves, and derive analytical
26 solutions by integrating over the canopy layer. To model leaf-level and canopy-level photosynthesis, leaf
27 light absorption is then linked to the biochemical process of gas diffusion through leaf stomata. The canopy
28 gap probability derived from GORT differs from classic radiative transfer theory, especially when the leaf
29 area index is high, due to leaf clumping effects. Tree characteristics such as tree density, crown shape, and
30 canopy length affect leaf clumping and regulate radiation interception. Modeled gross primary production
31 (GPP) for two deciduous forest stands could explain more than 80% of the variance of flux tower
32 measurements at both near hourly and daily time scales. ~~We also demonstrate that the ambient CO₂~~
33 ~~concentration influences daytime vegetation photosynthesis, which needs to be considered in state-of-the-art~~
34 ~~biogeochemical models. We demonstrate that ambient CO₂ concentrations influence daytime vegetation~~
35 ~~photosynthesis, which needs to be considered in biogeochemical models.~~ The proposed model is
36 complementary to classic radiative transfer theory and shows promise in modeling the radiative transfer
37 process and photosynthetic activities over discontinuous forest canopies.

38

39 Key words: gross primary production; flux tower; carbon cycle; radiative transfer; carbon assimilation

40 **1. Introduction**

41 Terrestrial plants assimilate atmospheric carbon dioxide through photosynthesis (Keenan et al., 2013;
42 Myneni et al., 1997). The climate system, in turn, affects vegetation development and photosynthetic
43 activities (Broich et al., 2014; Xia et al., 2014; Yi et al., 2010). Photosynthesis, accompanied by exchanges
44 of heat, water vapor, and trace gases within the planetary boundary layer, modifies microclimates and local
45 environments and determines ecosystem functions and services (Peng et al., 2014; Xu et al., 2013). The
46 complex biosphere/atmosphere feedbacks are dynamic and interactive (Bonan, 2008; Heimann and
47 Reichstein, 2008), such that robust numerical models that simulate vegetation photosynthesis are required in
48 terrestrial ecosystem models to understand the global carbon cycle (Cramer et al., 2001; Kucharik et al.,
49 2006).

50

51 Vegetation photosynthesis activity is regulated by environmental factors, and the light environment within
52 plant canopies is one of the key drivers (Law et al., 2002; Pearcy and Sims, 1994). Biophysical models such
53 as Production Efficiency Models assume linear relationships between absorbed photosynthetically active
54 radiation (APAR) and vegetation primary production (Field et al., 1995; Monteith, 1977; Potter et al., 1993;
55 Prince and Goward, 1995; Running et al., 2000). Because vegetation photosynthesis harvests solar radiation
56 by green chlorophyll, recent studies have attempted to quantify the fractions of APAR that are absorbed by
57 green chlorophyll (Zhang et al., 2014; Zhang et al., 2005). Physiologically, plants assimilate carbon dioxide
58 via the biochemical diffusion processes through stomata, numerous small pores on the leaf surfaces (Collatz
59 et al., 1991; Farquhar and Sharkey, 1982). Stomata can open and close in response to microenvironments,
60 thereby regulating plant carbon uptake (Bonan, 2002). Field physiological studies have accumulated
61 detailed information on the behavior of stomata under certain environmental conditions (Schulze et al.,
62 1994), in which sunlight irradiance plays a vital role (Ball et al., 1987). In this domain, linking the physical
63 process of radiative transfer within plant canopies with the biochemical process of gas diffusion through leaf
64 stomata is essential for accurate representation of vegetation photosynthesis.

66 Radiative transfer within a plant canopy is determined by many factors such as the partition of incoming
67 solar radiation, solar illumination geometry, terrain slope and aspects, canopy structure, leaf angle
68 distribution, and leaf and substrate spectral properties (Baldocchi et al., 1985; Fan et al., 2014; Schaaf et al.,
69 1994). Classic radiative transfer theory assumes that plant leaves are randomly distributed in three-
70 dimensional space within a homogeneous canopy layer (Goudriaan, 1977; Myneni et al., 1990). The canopy
71 radiative transfer process can be simply characterized by leaf area index (LAI) and leaf angle distribution
72 (LAD). Three-dimensional, multi-layer, and two-leaf radiative transfer models have been developed to
73 simulate leaf absorption of solar irradiance and canopy photosynthesis (Myneni, 1991; Pury and Farquhar,
74 1997; Ryu et al., 2011; Sellers, 1985). Although classic radiative transfer theory holds well for dense
75 vegetation canopies, most vegetation canopies, especially arboreal canopies, consist of discrete crowns in
76 reality (Yuan et al., 2013). Leaves are clumped within individual crowns, such that more sunlight penetrates
77 to understory layers and the ground surfaces (He et al., 2012; Ni-Meister et al., 2010). Tree crowns also cast
78 shadows on one another and on the background, resulting in self-shadowing effects as described by the
79 geometric-optical theory (Li and Strahler, 1992). Given natural differences in the radiative transfer process
80 between homogenous and discontinuous plant canopies, it is important to understand and account for the
81 influence of crown shape and tree structure on canopy radiation absorption and vegetation photosynthesis.

82

83 To address the radiative transfer process in discontinuous canopies, the Geometric-Optical Radiative-
84 Transfer (GORT) model conceptually combines geometric optical principles for canopy structure and
85 radiative transfer theory for volumetric scattering within canopy crowns (Li et al., 1995). The geometric
86 optical method is used to characterize the process by which sunlight passes directly to the ground surface
87 without reaching any canopy crowns. The radiative transfer principle is applied to model the probability of
88 light penetration as it travels through crowns in the canopy. GORT has been used to model the physical
89 aspects of discontinuous plant canopies such as gap fraction, radiation transmission, and bi-directional

90 reflectance (Ni et al., 1999; Ni et al., 1997; Xin et al., 2012), and has been validated under a variety of
91 environmental conditions (Liu et al., 2008). Recent efforts have been made to develop and evaluate a
92 simplified GORT model for the use in coupled global dynamic terrestrial ecosystem models (Ni-Meister et
93 al., 2010; Yang et al., 2010). Despite these successful applications, the current version of the GORT model
94 does not have analytical solutions for radiation absorption by sunlit and shaded leaves, though previous
95 studies have tried to solve the process of multiple scattering between canopy and background in an iterative
96 manner (Song et al., 2009). However, sunlit and shaded leaves must be treated separately in photosynthesis
97 modeling because flux densities of photosynthetically active radiation (PAR) incident on leaf surfaces are
98 different (He et al., 2013). It is also necessary to integrate vertically over the canopy to derive mean PAR
99 absorbed by sunlit and shaded leaves because of the non-linear light attenuation within the canopy and the
100 non-linear dependence of leaf stomatal conductance on light absorption (Campbell and Norman, 1998).

101

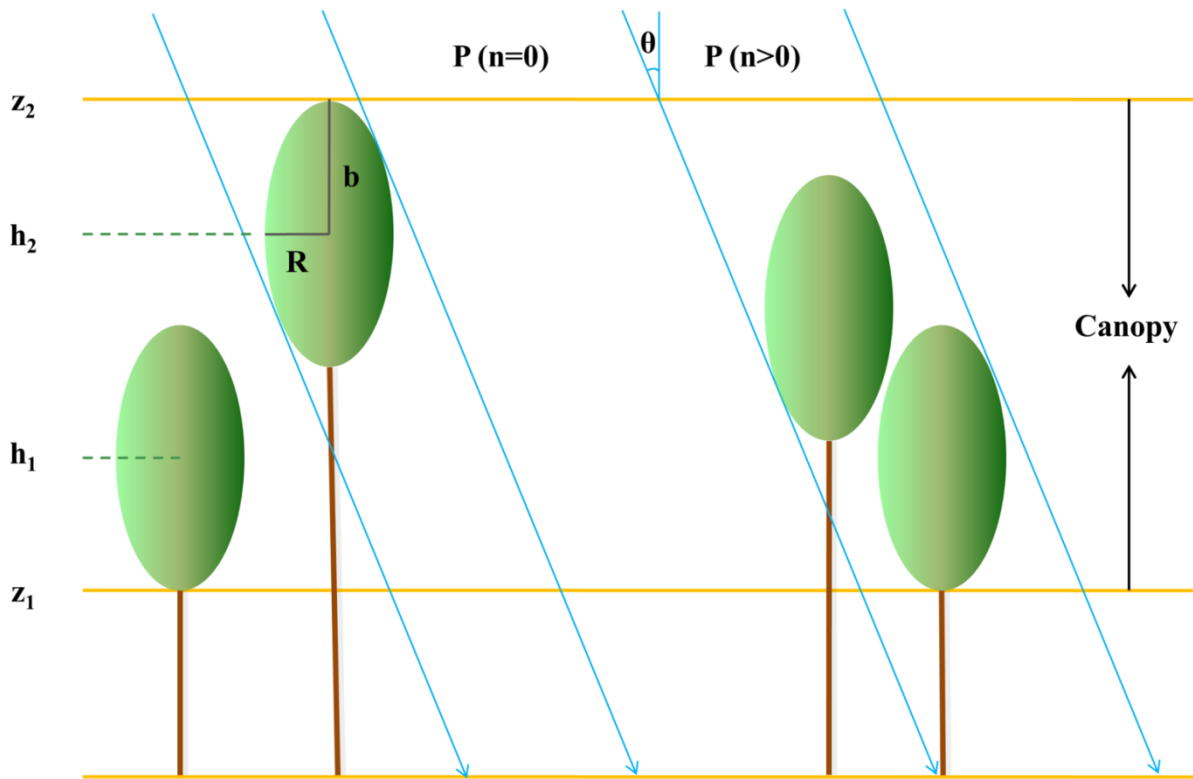
102 The objectives of this study are to 1) advance the GORT model by providing analytical solutions to the
103 radiation absorption of sunlit and shaded leaves and 2) link the radiative transfer process to biochemical
104 processes to simulate leaf and canopy photosynthesis. We first describe the principles of our model and then
105 perform model validation with eddy covariance data from two flux towers situated in the New England
106 region of the United States.

107

108 **2. Theoretical Basis**

109 **2.1 Brief description of canopy gap probability modeled using GORT**

110 Gap probability, the probability of photons reaching a given canopy depth without being intercepted by
111 canopy elements, is key to characterizing the radiation distribution within plant canopies. A detailed
112 description for modeling the gap probability with GORT is described in previous studies (Li et al., 1995; Ni
113 et al., 1999), and we summarize it briefly here because the concept of gap probability is necessary for
114 understanding our subsequent work.



115

116 Figure 1: A scheme of the canopy structure in the Geometric Optical Radiative Transfer model as modified
 117 from Ni (1998).

118

119 For homogeneous canopies, Beer's law describes the gap probability of sunlight penetration. For
 120 discontinuous plant canopies, leaves are clumped within individual canopy crowns, forming an uneven
 121 distribution of gap probabilities for beam radiation. GORT models tree crowns as a collection of ellipsoids
 122 (Figure 1), of which the centers are randomly distributed between the upper and lower boundaries of the
 123 canopy layer (h_1 and h_2). Each ellipsoid, or each canopy crown, is characterized by one-half of the vertical
 124 crown length (b) and a horizontal crown radius (R). The total gap probability is modeled separately as the
 125 proportion of sunlight passing through the canopy layer without reaching any crown (hereafter referred to as
 126 between-crown gaps) and the proportion of sunlight passing through crowns without being intercepted by
 127 canopy leaves (hereafter referred to as within-crown gaps), such that:

	$P_{\text{gap}}(h, \theta_i) = P_{\text{gap}}(n = 0 h, \theta_i) + P_{\text{gap}}(n > 0 h, \theta_i)$	(1)
--	---	-----

128 where $P_{\text{gap}}(h, \theta_i)$ is the gap probability for beam radiation at height h given an illumination zenith angle θ_i ,
 129 $P_{\text{gap}}(n = 0|h, \theta_i)$ is the between-crown gap, and $P_{\text{gap}}(n > 0|h, \theta_i)$ is the within-crown gap.

130

131 The between-crown gap is modeled based on Boolean theory as an exponential function of crown numbers
 132 within a geometric volume that contains no crown centers:

$$P_{\text{gap}}(n = 0|h, \theta_i) = e^{-\lambda_v V_\Gamma} \quad (2)$$

133 where λ_v is the tree density, and V_Γ is the beam projected cylinder volume with a radius R starting from the
 134 canopy top and extending to height h .

135

136 Assuming that leaves are randomly distributed within each individual crown, the within-crown gap is
 137 modeled based on Beer's law as light penetration along the traveling path length, such that:

$$P_{\text{gap}}(n > 0|h, \theta_i) = \int_0^\infty P(s|h, \theta_i) e^{-\tau(\theta_i)s} ds \quad (3)$$

138 where $\tau(\theta_i, \alpha) = k_b(\theta_i, \alpha) \cdot \text{FAVD}$, FAVD is the foliage area volume density within a single crown, and
 139 $k_b(\theta_i, \alpha)$ is the extinction coefficient for beam radiation given a specific solar illumination angle θ_i and leaf
 140 distribution angle α . For a spherical leaf angle distribution, $k_b = \frac{0.5}{\cos(\theta_i)}$. $P(s|h, \theta_i)$ is the probability
 141 distribution function associated with within-crown path length s .

142

143 The probability distribution of within-crown paths length can be solved in a convolutional manner:

$$P(s|h, \theta_i) = \int_h^{h_2} \sum_{n=1}^{n=\infty} P(s|n, z, h, \theta_i) P(n|z, h, \theta_i) dz \quad (4)$$

144 where $P(s|n, z, h, \theta_i)$ is the probability distribution of within-crown path length given that a solar ray enters
 145 the crown at height h and angle θ_i , and $P(n|z, h, \theta_i)$ is the probability distribution of the numbers of crowns
 146 intercepted by the solar ray incident at angle θ_i , entering crowns at height z , and then traveling to height h .

147

148 Diffuse radiation (i.e., the hemispherically isotropic radiation) can be treated as beam radiation from all
 149 directions in the upper hemisphere. The “openness” of discontinuous plant canopies to diffuse radiation on a
 150 horizontal plane is defined as:

	$K_{\text{open}}(h) = K_{\text{open}}(n = 0 h) + K_{\text{open}}(n > 0 h)$	(5)
	$K_{\text{open}}(n = 0 h) = \frac{1}{\pi} \int_0^{2\pi} \int_0^{\frac{\pi}{2}} P_{\text{gap}}(n = 0 h, \theta_i) \sin(\theta_i) \cos(\theta_i) d\theta_i d\phi$ $= 2 \int_0^{\frac{\pi}{2}} P_{\text{gap}}(n = 0 h, \theta_i) \sin(\theta_i) \cos(\theta_i) d\theta_i$	(6)
	$K_{\text{open}}(n > 0 h) = \frac{1}{\pi} \int_0^{2\pi} \int_0^{\frac{\pi}{2}} P_{\text{gap}}(n > 0 h, \theta_i) \sin(\theta_i) \cos(\theta_i) d\theta_i d\phi$ $= 2 \int_0^{\frac{\pi}{2}} P_{\text{gap}}(n > 0 h, \theta_i) \sin(\theta_i) \cos(\theta_i) d\theta_i$	(7)

151 where $K_{\text{open}}(n = 0|h)$ and $K_{\text{open}}(n > 0|h)$ are between-crown and within-crown openness factors,
 152 respectively. θ_i is the solar illumination angle, and ϕ is the azimuth angle.

153

154 2.2 Sunlit and shaded leaf area index

155 The gap probability describes the probability of beam radiation being intercepted by plant leaves, and hence
 156 determines the proportion of leaf areas that are sunlit. For a very thin layer, the reduction of total gap
 157 probability is due to leaf interception, of which the process still follows Beer’s law:

	$P_{\text{gap}}(h - \delta h, \theta_i) = \exp(-k_b \delta LAI(h)) P_{\text{gap}}(h, \theta_i)$	(8)
--	---	-----

158 where k_b is the canopy extinction coefficient for beam irradiance, $\delta LAI(h)$ is the leaf area index within a
 159 thin layer δh at height h , and $P_{\text{gap}}(h, \theta_i)$ is the gap probability modeled using GORT.

160

161 In the limit as δh becomes infinitely small, we have:

	$\exp(-k_b \delta LAI(h)) = 1 - k_b \delta LAI(h)$	(9)
	$P_{\text{gap}}(h - \delta h, \theta_i) = P_{\text{gap}}(h, \theta_i) - P'_{\text{gap}}(h, \theta_i) \delta h$	(10)

162 where $P'_{\text{gap}}(h, \theta_i)$ is the first derivative of gap probability $P_{\text{gap}}(h, \theta_i)$ with respect to height h .

163

164 Combining Equations (8), (9), and (10), we obtain:

	$\frac{P'_{\text{gap}}(h, \theta_i)}{P_{\text{gap}}(h, \theta_i)} \delta h = k_b \delta LAI(h)$	(11)
--	---	------

165

166 For diffuse radiation, it can be derived in a similar manner:

	$\frac{K'_{\text{open}}(h)}{K_{\text{open}}(h)} \delta h = k_d \delta LAI(h)$	(12)
--	---	------

167 where k_d is the extinction coefficient for diffuse irradiance, and $K'_{\text{open}}(h)$ is the first derivative of the

168 openness factor $K_{\text{open}}(h)$ with respect to height h .

169

170 The sunlit LAI at height h is the product of the probability of beam sunlight penetration to height h and the

171 probability of sunlight being intercepted by the thin layer and divided by the ratio of leaf area projected on a

172 horizontal surface (Campbell and Norman, 1998), such that:

	$\delta LAI_{\text{sun}}(h, \theta_i) = \frac{P_{\text{gap}}(h, \theta_i) [1 - \exp(-k_b \delta LAI(h))]}{k_b}$	(13)
--	---	------

173 where $\delta LAI_{\text{sun}}(h, \theta_i)$ is the sunlit leaf area index within a thin layer δh at height h .

174

175 Substituting Equations (9) and (11) into Equation (13), we obtain:

$$\delta LAI_{Sun}(\theta_i) = \frac{P'_{\text{gap}}(h, \theta_i)}{k_b} \delta h \quad (14)$$

176

177 Sunlit LAI for the entire canopy at zenith angle θ is then obtained by integrating from the canopy top to
 178 canopy bottom, such that:

$$LAI_{Sun}(\theta_i) = \int_{z_1}^{z_2} \frac{P'_{\text{gap}}(h, \theta_i)}{k_b} dh = \frac{1 - P_{\text{gap}}(h = z_1 | \theta_i)}{k_b} \quad (15)$$

179 where $P_{\text{gap}}(h = z_2 | \theta_i)$ and $P_{\text{gap}}(h = z_1 | \theta_i)$ are the gap probabilities at the canopy top z_2 and canopy
 180 bottom z_1 , respectively, whereas the gap probability at the canopy top is 1.

181

182 It is worth noting that our calculation of sunlit leaf area for discontinuous canopies is analogous to that for
 183 homogeneous canopies, which is given as:

$$LAI_{Sun}^*(\theta_i) = \int_0^{LAI} \exp(-k_b \cdot L) dL = \frac{1 - \exp(-k_b \cdot LAI)}{k_b} \quad (16)$$

184 where $LAI_{Sun}^*(\theta_i)$ is the sunlit leaf area for homogeneous canopies.

185

186 The shaded LAI is simply the remainder of the canopy LAI:

$$LAI_{Shd} = LAI - LAI_{Sun} \quad (17)$$

187

188 2.3 Analytical solutions for the scattering parameters of discontinuous canopies

189 Canopy scattering parameters such as directional-hemispherical reflectance and hemispherical-
 190 hemispherical reflectance (or black-sky albedo and white-sky albedo, respectively) can be obtained by
 191 resolving the radiative transfer process or can be approximated using simple analytical solutions. For semi-
 192 infinite horizontally homogeneous media, Hapke's solutions of the proportion of unintercepted direct beam
 193 ($t_0(h, \theta_i)$), hemispherical-hemispherical reflectance (R_{ff}^∞), directional-hemispherical reflectance (R_{df}^∞),

194 hemispherical-hemispherical transmittance (T_{ff}^{∞}), and directional-hemispherical transmittance (T_{df}^{∞}) are
 195 given as (Hapke, 1981):

	$t_0(h, \theta_i) = e^{-\frac{\tau(\theta_i)h}{\mu_i}}$	(18)
	$R_{ff}^{\infty} = \frac{1 - \gamma}{1 + \gamma}$	(19)
	$R_{df}^{\infty}(\theta_i) = \frac{1 - \gamma}{1 + 2\mu_i\gamma}$	(20)
	$T_{ff}^{\infty}(h) = e^{-2\gamma\tau h}$	(21)
	$T_{df}^{\infty}(h, \theta_i) = \frac{\sigma}{2} \frac{1 + 2\mu_i}{1 - (2\mu_i\gamma)^2} [T_{ff}^{\infty}(h) - t_0(h, \theta_i)]$	(22)

196 where σ is the single scattering albedo, $\tau = k(\theta_i) \frac{L_e}{H}$ is the projected foliage area volume density for the
 197 plant canopy, L_e is the effective leaf area index, H is the depth of the canopy, θ_i is the solar illumination
 198 angle, $\mu_i = \cos(\theta_i)$ and $\gamma = \sqrt{1 - \sigma}$.

199

200 Starting with surface energy balances, Ni (1998) derived the scattering parameters for a horizontally
 201 homogeneous canopy layer with finite thickness as:

	$t_{ff}(h) = T_{ff}^{\infty}(h) \frac{1 - (R_{ff}^{\infty})^2}{1 - (T_{ff}^{\infty}(h)R_{ff}^{\infty})^2}$	(23)
	$\rho_{ff}(h) = R_{ff}^{\infty}(h) \frac{1 - (T_{ff}^{\infty}(h))^2}{1 - (T_{ff}^{\infty}(h)R_{ff}^{\infty})^2}$	(24)
	$t_{df}(h, \theta_i) = T_{df}^{\infty}(h, \theta_i) - \rho_{ff}(h)[t_0(h, \theta_i)R_{df}^{\infty}(\theta_i) + T_{df}^{\infty}(h, \theta_i)R_{ff}^{\infty}]$	(25)
	$\rho_{df}(h, \theta_i) = R_{df}^{\infty}(h) - t_{ff}(h)[t_0(h, \theta_i)R_{df}^{\infty}(\theta_i) + T_{df}^{\infty}(h, \theta_i)R_{ff}^{\infty}]$	(26)

202 where $t_{ff}(h)$, $\rho_{ff}(h)$, $t_{df}(h, \theta_i)$, and $\rho_{df}(h, \theta_i)$ are hemispherical-hemispherical transmittance,
 203 hemispherical-hemispherical reflectance, directional-hemispherical transmittance, and directional-
 204 hemispherical reflectance, respectively.

205

206 The scattering parameters for a discontinuous canopy can then be approximated as combinations of a
 207 homogeneous vegetation layer and a non-vegetated layer:

	$t'_{ff}(h) = t_{ff}(h) (1 - K_{\text{open}}(n = 0 h)) + K_{\text{open}}(n = 0 h)$	(27)
	$\rho'_{ff}(h) = \rho_{ff}(h) (1 - K_{\text{open}}(n = 0 h))$	(28)
	$t'_{df}(h, \theta_i) = t_{df}(h, \theta_i)(1 - P_{\text{gap}}(n = 0 h, \theta_i)) + P_{\text{gap}}(n = 0 h, \theta_i)$	(29)
	$\rho'_{df}(h, \theta_i) = \rho_{df}(h, \theta_i)(1 - P_{\text{gap}}(n = 0 h, \theta_i))$	(30)

208 where $t'_{ff}(h)$, $\rho'_{ff}(h)$, $t'_{df}(h, \theta_i)$, and $\rho'_{df}(h, \theta_i)$ are hemispherical-hemispherical transmittance,
 209 hemispherical-hemispherical reflectance, directional-hemispherical transmittance, and directional-
 210 hemispherical reflectance, respectively. Note that our equations here are slightly different from those used
 211 by Ni et al. (1999) because between-crown gaps, within which light attenuation obeys Beer's law, are
 212 considered in the homogeneous vegetation layer.

213

214 The analytical approximation of the canopy reflectance for beam and diffuse radiation is the sum of three
 215 factors in radiative transfer: the incoming irradiance scattered by the canopy elements, the first-order
 216 scattered radiation from soil background, and the irradiance scattered back and forth between the canopy
 217 layer and background surface (Ni et al., 1999). Taking beam radiation as an example and assuming that the
 218 background surface is Lambertian, the incoming irradiance scattered by the canopy elements is ρ'_{df} , the
 219 first-order scattered radiance from soil background is $t'_{df}\rho_s t'_{ff}$, and the multiple scattering between the

220 canopy elements and soil background is $t'_{df}(\rho_s \rho'_{ff} \rho_s + \rho_s (\rho'_{ff} \rho_s)^2 + \rho_s (\rho'_{ff} \rho_s)^3 + \dots) t'_{ff}$. The canopy
 221 reflectance for beam irradiance can then be written as:

	$\rho_{cb} = \rho'_{df} + t'_{df}(\rho_s + \rho_s \rho'_{ff} \rho_s + \rho_s (\rho'_{ff} \rho_s)^2 + \rho_s (\rho'_{ff} \rho_s)^3 + \dots) t'_{ff}$ $= \rho'_{df} + t'_{df} \frac{\rho_s}{1 - \rho_s \rho'_{ff}} t'_{ff}$	(31)
--	---	------

222
 223 The canopy reflectance for diffuse irradiance can be obtained similarly as:

	$\rho_{cd} = \rho'_{ff} + t'_{ff} \frac{\rho_s}{1 - \rho_s \rho'_{ff}} t'_{ff}$	(32)
--	---	------

224
 225 **2.4 Mean photosynthetically active radiation absorbed by sunlit and shaded leaves**

226 Let I_0 be the flux density of incoming solar radiation on a horizontal plane at the top of the canopy and f_b be
 227 the fraction of incident beam radiation, the unintercepted beam and diffuse fluxes are then:

	$I_b(h, \theta_i) = P_{\text{gap}}(h, \theta_i)(1 - \rho_{cb})f_b I_0 k_b$	(33)
	$I_d(h) = K_{\text{open}}(h)(1 - \rho_{cd})(1 - f_b)I_0 k_d$	(34)

228 where ρ_{cb} and ρ_{cd} are canopy reflectance for beam and diffuse irradiance, respectively; I_b and I_d are the
 229 unintercepted beam and diffuse fluxes, respectively; and k_b and k_d are canopy extinction coefficients for
 230 beam and diffuse irradiance, respectively.

231
 232 The downward beam flux I_b is derived based on the assumption of black leaves, meaning that leaves absorb
 233 incident irradiance completely and do not transmit radiation (Bonan, 2002). To account for the effects of
 234 leaf scattering, the total beam I_{bt} (i.e., unintercepted beam and down scattered beam) and total diffuse I_{dt}
 235 (i.e., unintercepted diffuse and down scattered diffuse) irradiance can be modeled by introducing a factor of
 236 $\sqrt{1 - \sigma}$ to extinction coefficients similar to the two-stream radiative transfer model (Sellers, 1985). As

237 single scattering albedo increases, the effective extinction coefficient becomes smaller and more sunlight is
 238 allowed to transmit through the canopy. That is:

	$I_{bt}(h, \theta_i) = P_{\text{gap}}(h, \theta_i)^{\sqrt{1-\sigma}}(1 - \rho_{cb})f_b I_0 \sqrt{1 - \sigma} k_b$	(35)
--	---	------

	$I_{dt}(h) = K_{\text{open}}(h)^{\sqrt{1-\sigma}}(1 - \rho_{cd})(1 - f_b)I_0 \sqrt{1 - \sigma} k_d$	(36)
--	---	------

239 where σ is the single scattering albedo of leaves. $\sigma = \rho_l + t_l$, where ρ_l and t_l are leaf reflectance and
 240 transmittance, respectively.

241

242 The total irradiance absorbed by the entire canopy per unit ground area consists of leaf absorption for both
 243 beam and diffuse irradiance:

	$I_c = I_{cb} + I_{cd} = \int_0^{LAI} I_{bt}(h, \theta_i) dL + \int_0^{LAI} I_{dt}(h, \theta_i) dL$	(37)
--	---	------

244

245 Substituting Equations (11), (12), (35), and (36) into Equation (37), we have:

	$I_{cb} = \int_{z_1}^{z_2} P_{\text{gap}}(h, \theta_i)^{\sqrt{1-\sigma}}(1 - \rho_{cb})f_b I_0 \sqrt{1 - \sigma} \frac{P'_{\text{gap}}(h, \theta_i)}{P_{\text{gap}}(h, \theta_i)} dh$ $= (1 - P_{\text{gap}}(h = z_1 \theta_i)^{\sqrt{1-\sigma}})(1 - \rho_{cb})f_b I_0$	(38)
--	---	------

	$I_{cd} = \int_{z_1}^{z_2} K_{\text{open}}(h)^{\sqrt{1-\sigma}}(1 - \rho_{cd})(1 - f_b)I_0 \sqrt{1 - \sigma} \frac{K'_{\text{open}}(h)}{K_{\text{open}}(h)} dh$ $= (1 - K_{\text{open}}(h = z_1)^{\sqrt{1-\sigma}})(1 - \rho_{cd})(1 - f_b)I_0$	(39)
--	--	------

246

247 Irradiance absorbed by sunlit leaves per unit ground area is obtained as the sum of direct beam, downward
 248 scattered beam, and diffuse components:

	$I_{\text{sun}} = I_{\text{sunb}} + I_{\text{sunbs}} + I_{\text{sund}}$	(40)
--	---	------

249

250 Combining Equations (33), (35), (36), and (40), we have:

$$I_{Sunb} = \int_{z_1}^{z_2} (1 - \sigma) f_b I_0 \cdot P'_{\text{gap}}(h, \theta_i) dh = (1 - \sigma) \left(1 - P_{\text{gap}}(h = z_1 | \theta_i)\right) f_b I_0 \quad (41)$$

$$\begin{aligned} I_{Sunbs} &= \int_{z_1}^{z_2} [P_{\text{gap}}(h, \theta_i)^{\sqrt{1-\sigma}} (1 - \rho_{cb}) \sqrt{1-\sigma} - P_{\text{gap}}(h, \theta_i) (1 - \sigma)] f_b I_0 \cdot P'_{\text{gap}}(h, \theta_i) dh \\ &= \left[\frac{\sqrt{1-\sigma}}{1 + \sqrt{1-\sigma}} (1 - P_{\text{gap}}(h = z_1 | \theta_i)^{1+\sqrt{1-\sigma}}) (1 - \rho_{cb}) \right. \\ &\quad \left. - \frac{(1-\sigma)}{2} (1 - P_{\text{gap}}(h = z_1 | \theta_i)^2) \right] f_b I_0 \end{aligned} \quad (42)$$

$$\begin{aligned} I_{Sund} &= \int_{z_1}^{z_2} K_{\text{open}}(h)^{\sqrt{1-\sigma}} (1 - \rho_{cd}) (1 - f_b) I_0 \sqrt{1-\sigma} \cdot K'_{\text{open}}(h) dh \\ &= \frac{\sqrt{1-\sigma}}{1 + \sqrt{1-\sigma}} (1 - K_{\text{open}}(h = z_1)^{1+\sqrt{1-\sigma}}) (1 - \rho_{cd}) (1 - f_b) I_0 \end{aligned} \quad (43)$$

251 Note that σ is used instead of ρ_{cd} for the beam irradiance of sunlit leaves because sunlit leaves scatter direct
252 beam sunlight only once.

253

254 The irradiance absorbed by shaded leaves per unit ground area is simply the difference between the total
255 irradiance absorbed by the canopy and the irradiance absorbed by sunlit leaves:

$$I_{Shd} = I_c - I_{Sun} \quad (44)$$

256

257 The mean absorbed irradiance for sunlit and shaded canopy per leaf hemi-surface area is then:

$$Q_{Sun} = \frac{I_{Sun}}{LAI_{Sun}} \quad (45)$$

$$Q_{Shd} = \frac{I_{Shd}}{LAI_{Shd}} \quad (46)$$

258

259 **2.5 Modeling leaf photosynthesis and scaling up to canopy photosynthesis**

260 The biochemical process of carbon dioxide assimilation by leaves can be considered as a gas diffusion
261 process through stomata. According to Fick's law, the process is described as:

	$A = g_c \cdot (C_a - C_i)$	(47)
--	-----------------------------	------

262 where A is the CO_2 assimilation rate, g_c is the stomatal conductance, and C_a and C_i are ambient and
263 intercellular CO_2 concentrations, respectively.

264

265 Field studies have firmly established the relationship between leaf stomatal conductance and environmental
266 conditions. Jarvis and McNaughton (1986) successfully synthesize the response functions in a multiple-
267 constraint model:

	$g_c = g_{cmax} \prod f(x_i)$	(48)
--	-------------------------------	------

268 where g_{cmax} is the maximum leaf stomatal conductance when environmental factors do not limit carbon
269 uptake and $f(x_i)$ are scalars that account for the influences of various environmental stresses on leaf
270 stomatal conductance.

271

272 Different formulas have been developed to describe the response functions of photosynthesis to
273 environmental factors. Here, we consider three main limiting factors imposed by radiation, temperature, and
274 water on vegetation photosynthesis. The equations developed for the dual-source dual-leaf (DSDL) model
275 (Ding et al., 2014), Terrestrial Ecosystem Model (Raich et al., 1991), and Biome-BGC models (Running et
276 al., 2004) are used to account for the influences of radiation, temperature, and vapor pressure deficit (VPD),
277 respectively:

	$\prod f(x_i) = f(Q) \cdot f(T) \cdot f(VPD)$	(49)
--	---	------

	$f(Q) = \frac{k_C + k_Q}{k_Q} \cdot \frac{Q}{k_Q + Q}$	(50)
	$f(T) = \frac{(T - T_{min})(T - T_{max})}{(T - T_{min})(T - T_{max}) - (T - T_{opt})^2}$	(51)
	$f(VPD) = \frac{VPD_{max} - VPD}{VPD_{max} - VPD_{min}}$	(52)

278 where k_C and k_Q are the stress coefficients of PAR absorbed by plant leaves; Q is the mean APAR for sunlit
279 or shaded leaves per leaf hemi-surface area; T_{min} , T_{opt} , and T_{max} are the minimum, optimum, and
280 maximum temperature for photosynthetic activities, respectively; and VPD_{min} and VPD_{max} are the
281 minimum and maximum vapor pressure deficit, respectively. In the DSDL model, k_C and k_Q are 500 W/m²
282 and 150 W/m², respectively. T_{min} , T_{opt} , and T_{max} are determined as 10 °C, 28 °C and 48 °C for C4 crops
283 (Kalfas et al., 2011), and here we slightly lower their values to 0 °C, 25 °C, and 45 °C, respectively, for C3
284 plants. VPD_{min} and VPD_{max} are 0.65 kPa and 4.6 kPa for deciduous forests, respectively, in the Biome-
285 BGC model (Heinsch et al., 2003).

286

287 Due to different PAR absorption by sunlit and shaded leaves, the stomatal conductance for sunlit and shaded
288 leaves need to be calculated separately as:

	$g_{cSun} = g_{cmax} \cdot f(Q_{Sun}) \cdot f(T) \cdot f(VPD)$	(53)
	$g_{cShd} = g_{cmax} \cdot f(Q_{Shd}) \cdot f(T) \cdot f(VPD)$	(54)

289 where g_{cSun} and g_{cShd} are the stomatal conductance for sunlit and shaded leaves, respectively, and Q_{Sun}
290 and Q_{Shd} are the mean PAR absorbed by sunlit and shaded leaves, respectively.

291

292 Given measured ambient CO_2 concentrations, the closure of the formulation (47) now requires the quantity
293 of intercellular CO_2 concentrations. Katul et al. (2000) compared eight models and concluded that all

294 reproduced the measured carbon assimilation rates well. Here, we employ Leuning's method (Leuning,
295 1995) to estimate the ratio of intercellular to ambient CO_2 concentrations as:

$$\frac{C_i}{C_a} = 1 - \frac{1 - \frac{\Gamma}{C_a}}{m_L} \left(1 + \frac{VPD}{VPD_0}\right) \quad (55)$$

296 where VPD is the ambient vapor pressure deficit; VPD_0 is an empirical constant describing the species
297 sensitivity to ambient vapor pressure deficit; Γ is the leaf CO_2 compensation point; C_a and C_i are ambient
298 and intercellular CO_2 concentrations, respectively; and m_L represents linear regression coefficients related
299 to tree species. Calibrated values for model parameters are $m_L = 4.0$, $\Gamma = 40 \mu\text{mol/mol}$, and $VPD_0 =$
300 30 kPa, respectively (Katul et al., 2000).

301

302 Given modeled carbon assimilation rates at the leaf level, the total rate of carbon assimilation at the canopy
303 level can be scaled up as:

$$GPP = A_{Sun} \cdot LAI_{Sun} + A_{Shd} \cdot LAI_{Shd} \quad (56)$$

304 where GPP is canopy gross primary production, A_{Sun} and A_{Shd} are leaf-level carbon assimilation rates for
305 sunlit and shaded leaves, respectively, and LAI_{Sun} and LAI_{Shd} are the sunlit and shaded leaf area index.

306

307 **3. Study materials and model parameterization**

308 We studied two deciduous forest sites: Harvard Forest (US-Ha1) in Massachusetts and Bartlett Experimental
309 Forest (US-Bar) in New Hampshire (Richardson et al., 2012). Basic information is briefly summarized in
310 Table 1 for each site. Although plot layouts set up for the fieldwork did not match the exact footprints of
311 flux towers (Yang et al., 2013), the measured tree structural attributes, such as tree density, are assumed to
312 be representative of the two study sites.

313

314

315 Table 1. Site information as obtained from the AmeriFlux website unless notified.

Site code	Site name	Lat (°N)	Lon (°W)	Elevation (m)	Canopy height (m)	Tree density (trees/ha) ^a	Dominant species
US-Ha1	Harvard Forest	42.5378	72.1715	340	23.0	1020±72	red oak, red maple
US-Bar	Bartlett Experimental Forest	44.0646	71.2881	272	19.0	1432±67	American beech, red maple

316 ^a data from Yao et al. (2011)

317

318 Flux towers measure energy and material fluxes between ecosystem and the atmosphere continuously
 319 (Baldocchi et al., 2001). Measured data are provided as standard Level 2 products in the AmeriFlux
 320 database (<http://ameriflux.ornl.gov/>). The time steps of available data are half-hourly for US-Bar and hourly
 321 for US-Ha1. The measurements we used include estimates of gross primary production (GPP) derived with
 322 the eddy covariance technique (Baldocchi, 2003), and meteorological variables such as shortwave solar
 323 radiation, temperature, vapor pressure deficit, and canopy-scale CO₂ concentration. Raw measurements of
 324 meteorological variables were used for analysis and missing values due to instrument malfunction or
 325 unsuitable micrometeorological conditions were screened. However, we obtained GPP estimates from
 326 AmeriFlux Level 4 products if they were not delivered in Level 2 products. Extraterrestrial solar radiation
 327 and solar zenith angle ([i.e., the angle that the sun away from directly overhead](#)) are calculated as a function
 328 of geolocation (i.e., latitude and longitude), the day of year (DOY), and solar time of the day (Allen et al.,
 329 1998). If diffuse radiation is missing from the measurements, we implement Muneer’s method to partition
 330 global solar radiation into beam and diffuse components (Muneer, 2007):

$(1 - f_b) = 1.006 - 0.317K_t + 3.1241K_t^2 - 12.7616K_t^3 + 9.7166K_t^4$	(57)
---	------

331 where f_b is the proportion of beam radiation in global incoming radiation, and K_t is the hourly clearness
 332 index. $K_t = I_0/I_e$, where I_0 is global solar radiation on the canopy top and I_e is the extraterrestrial solar
 333 radiation.

334

335 We use typical parameter values from the literature for model parameterization. Because the spectral
 336 signatures of vegetation leaves and soil background differ in the spectral bands of PAR and near infrared

337 (Table 2), we perform model simulations for these two discrete bands separately. Incident PAR is estimated
 338 to account for 47.5% of incoming shortwave solar radiation, and the rest is attributed to the near infrared
 339 band (Zhao et al., 2005). Maximum leaf stomatal conductance to H₂O is estimated as 5.5 mm/s for US-Bar
 340 and 7.2 mm/s for US-Ha1 (Bonan, 2002; Ding et al., 2014), and they are translated to maximum leaf
 341 stomatal conductance to CO₂ assuming that the temperature is 20°C and the atmospheric pressure is 101.32
 342 kPa (Pearcy et al., 1989). Heights for canopy top (z_2) were measured to be 23.0 m for US-Ha1 and 19.0 m
 343 for US-Bar (Table 1), and heights for canopy bottom (z_1) were estimated as $z_1 = 0.15 z_2$. Canopy structure
 344 in GORT is modeled with the ratios $H/b = 2.0$ and $b/R = 3.0$ (Strahler et al., 1999). Parameter values
 345 defined for canopy structure are somewhat arbitrary but are identical to our previous modeling efforts (Liu
 346 et al., 2008; Xin et al., 2012). The effects of tree structural parameters on model simulations are further
 347 explored in our study by varying their values.

348

349 Table 2. The spectral signature of leaf and soil background.

Spectral bands	Leaf reflectance ^a	Leaf transmittance ^a	Soil reflectance ^b
Photosynthetic active radiation	0.10	0.05	0.23
Near infrared	0.45	0.25	0.32

350 ^a data from Bonan (2002)

351 ^b data from Myneni et al. (1995)

352

353 Model validation for vegetation photosynthesis is performed with time series data for 8 successive days and
 354 for entire years. Based on AmeriFlux biological data, measured LAI were 4.7 ± 0.2 on DOY 211 in 2004 at
 355 the US-Bar site and 4.84 ± 0.78 on DOY 234 in 2006 at the US-Ha1 site. Because field-measured LAI data
 356 were insufficient to support model simulation for an entire calendar year, we obtained satellite-derived LAI
 357 from the ~~state-of-the-art~~ MODIS (Moderate Resolution Imaging Spectroradiometer) products (Myneni et al.,
 358 2002). The standard MODIS products (MOD15A2) provide 8-day LAI estimates at 1000 m spatial
 359 resolution, and we derived 8-day mean LAI for a 3×3 pixel window centered at each site. We screened
 360 cloudy observations based on the Quality Control data in MOD15A2 and applied double logistic equations
 361 to fit time series of cloud-free LAI observations (Li et al., 2014; Zhang et al., 2003).

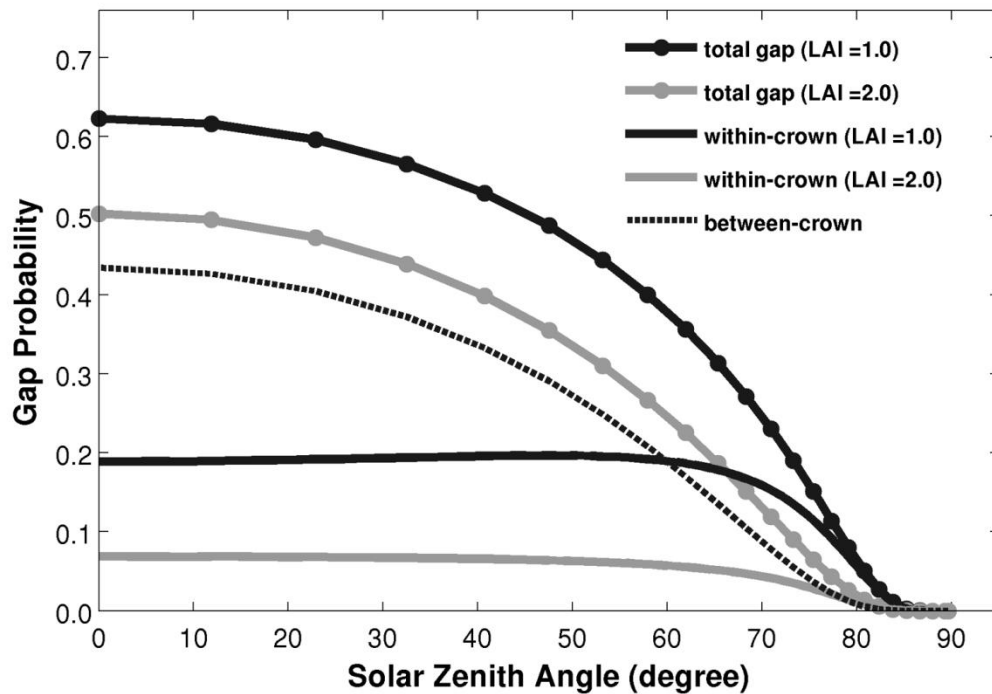
362

363 4. Results

364 4.1 Gap probability

365 The gap probabilities derived from the GORT model are shown in Figure 2. As the illumination-solar zenith
366 angle increases, more beams of sunlight are intercepted by leaves and tree crowns, resulting in decreased
367 gap probabilities for both between- and within-crown gaps. As LAI increases, within-crown gaps decrease
368 but between-crown gaps remain the same. The physical explanation underlying is simple: tree leaves are
369 clumped within each individual crown such that variations in LAI would not affect between-crown gaps,
370 which are only a function of crown shape, canopy structure, and illumination geometry.

371



372

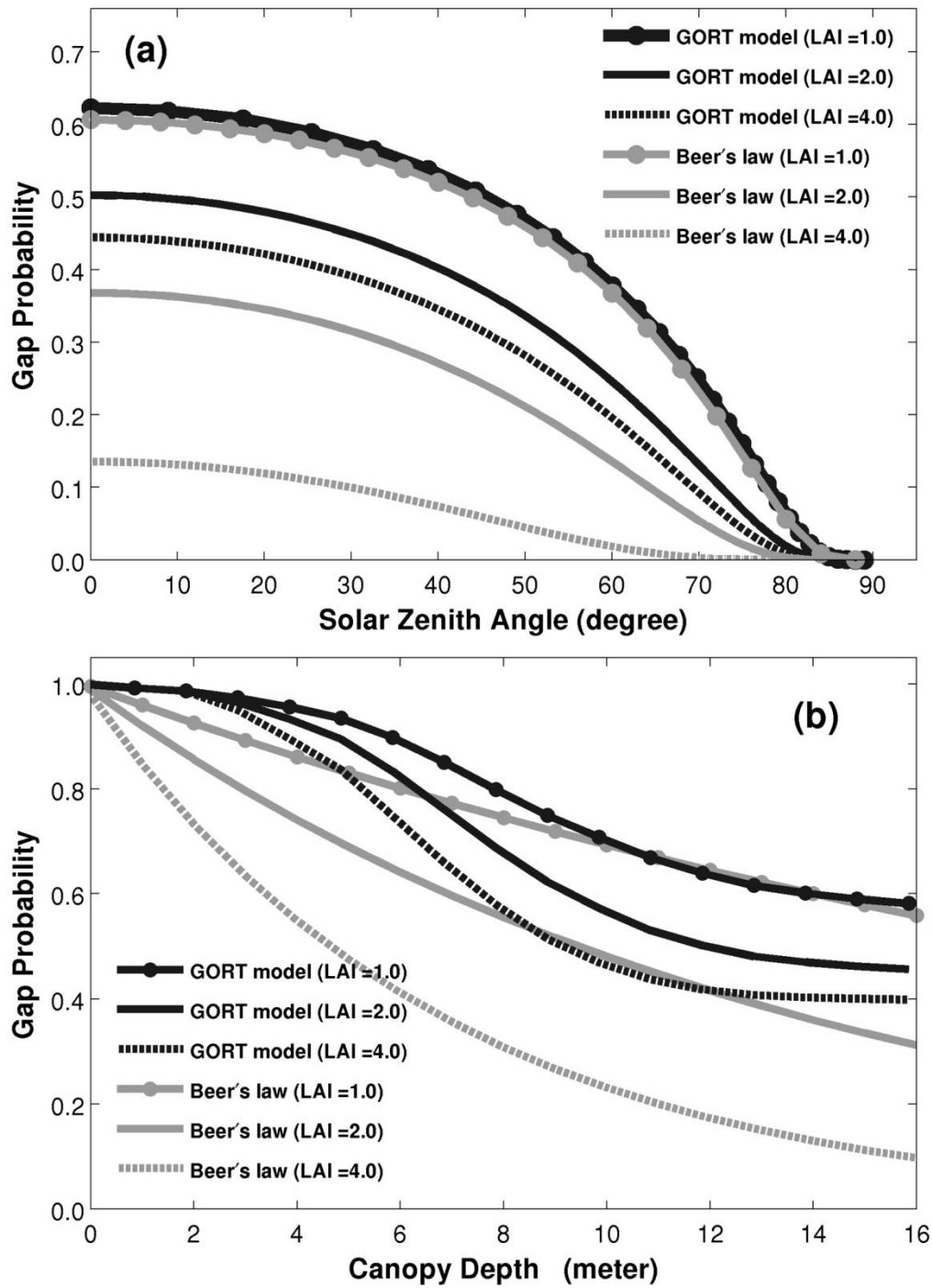
373 Figure 2: Canopy gap probabilities modeled using GORT with varied leaf area index. The total gaps are
374 between-crown gaps plus within-crown gaps. Tree structure parameters for the US-Bar site are used in
375 model simulation.

376

377 Figure 3 further compares the gap probabilities modeled using GORT and Beer's law. For both models, gap
378 probabilities decrease as solar zenith angle increases (Figure 3a). Modeled gap probabilities are close when

379 canopy LAI is low. However, at high LAI, the total gap derived from GORT is considerably greater than
380 that modeled using Beer's law due to strong clumping effects. With an LAI of 4.0, the differences in gap
381 probabilities are as much as 0.3 at the nadir, and in this case, more sunlight is allowed to transmit to the
382 ground surface in GORT than in classic radiative transfer models. Modeled vertical structures of sunlight
383 penetration are also shown to be different between GORT and Beer's law (Figure 3b). The gap probability
384 modeled using Beer's law decreases exponentially as canopy depth increases, whereas the decrease in the
385 GORT-modeled gap probability follows an inverse sigmoidal curve. The reason behind this can be
386 explained by the geometric factor: classic radiative transfer models assume that leaves are randomly
387 distributed within the canopy layer, but the GORT model assumes that leaves are randomly distributed
388 within individual crowns. Due to the ellipsoidal shape of tree crowns, there are simply more leaves in the
389 canopy center than near the canopy top and canopy bottom, where the gap probability decreases more
390 slowly.

391



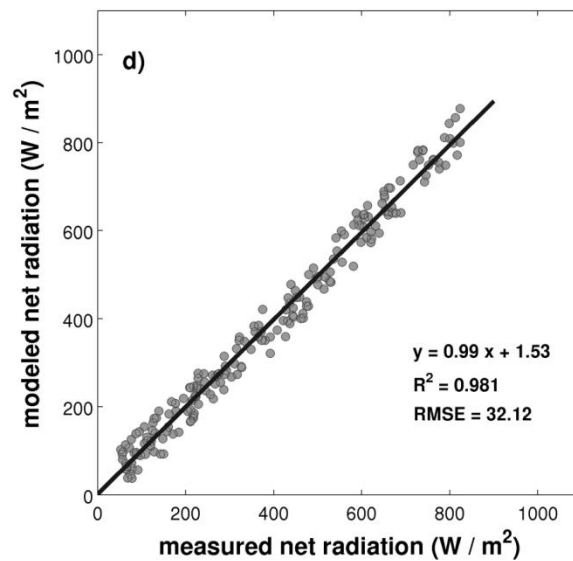
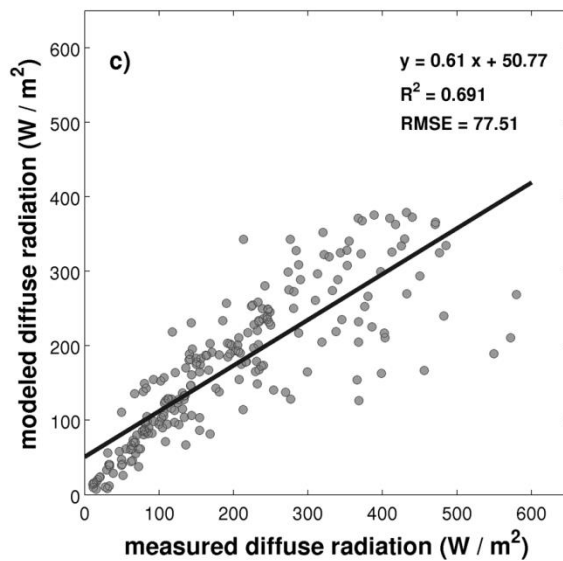
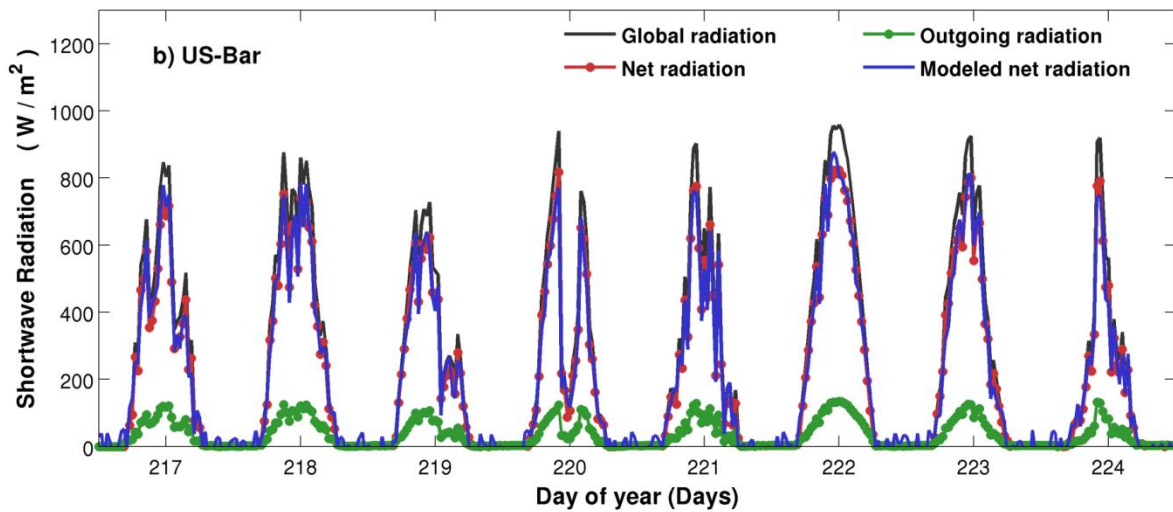
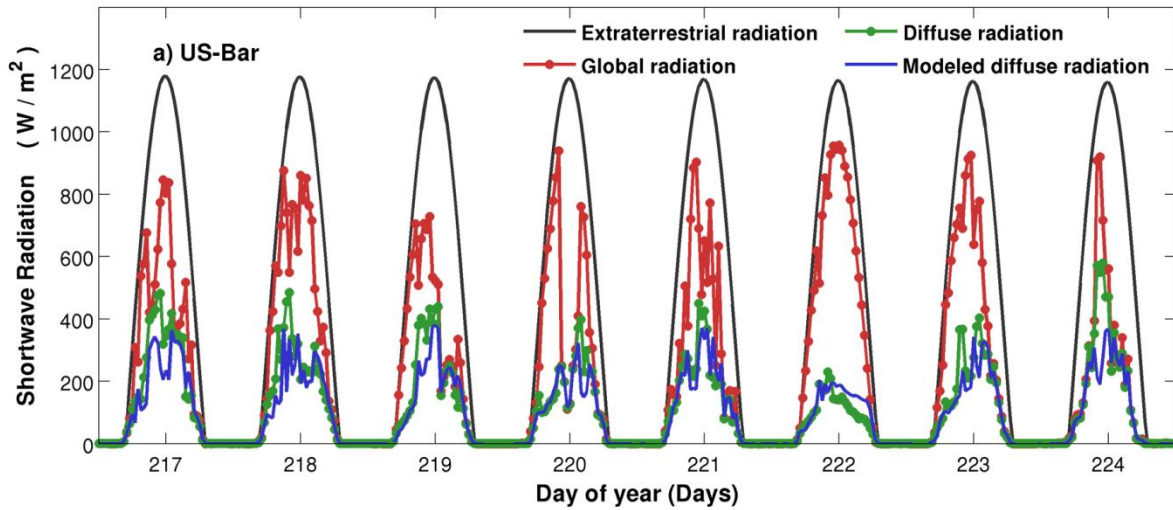
392

393 Figure 3: Comparisons between canopy gap probabilities modeled using GORT and Beer's law as a
 394 function of a) solar zenith angle and b) canopy depth. The canopy depth is defined as the distance from
 395 canopy top to a canopy height (h). Tree structure parameters for the US-Bar site are used in GORT
 396 simulation.

397

398 **4.2 Model simulations over 8-day time periods**

399 Figure 4 shows each component of the radiation regime at the US-Bar site. The diffuse radiation modeled
400 using Muneer's method matches flux tower measurements and accounts for ~~83.5%~~69.1% of the variances
401 (Figure 4a). Because diffuse radiation was not measured at the US-Ha1 site, Muneer's method was
402 implemented to partition global radiation into diffuse and beam components for US-Ha1. Using the
403 measured beam and diffuse radiation, we simulate net radiation with GORT as a linear combination of two
404 discrete bands at PAR and near infrared. Modeled net radiation is highly correlated with measured values
405 ($R^2=\del{0.998}0.981), demonstrating the ability of GORT to model radiation absorption at the US-Bar site.
406$



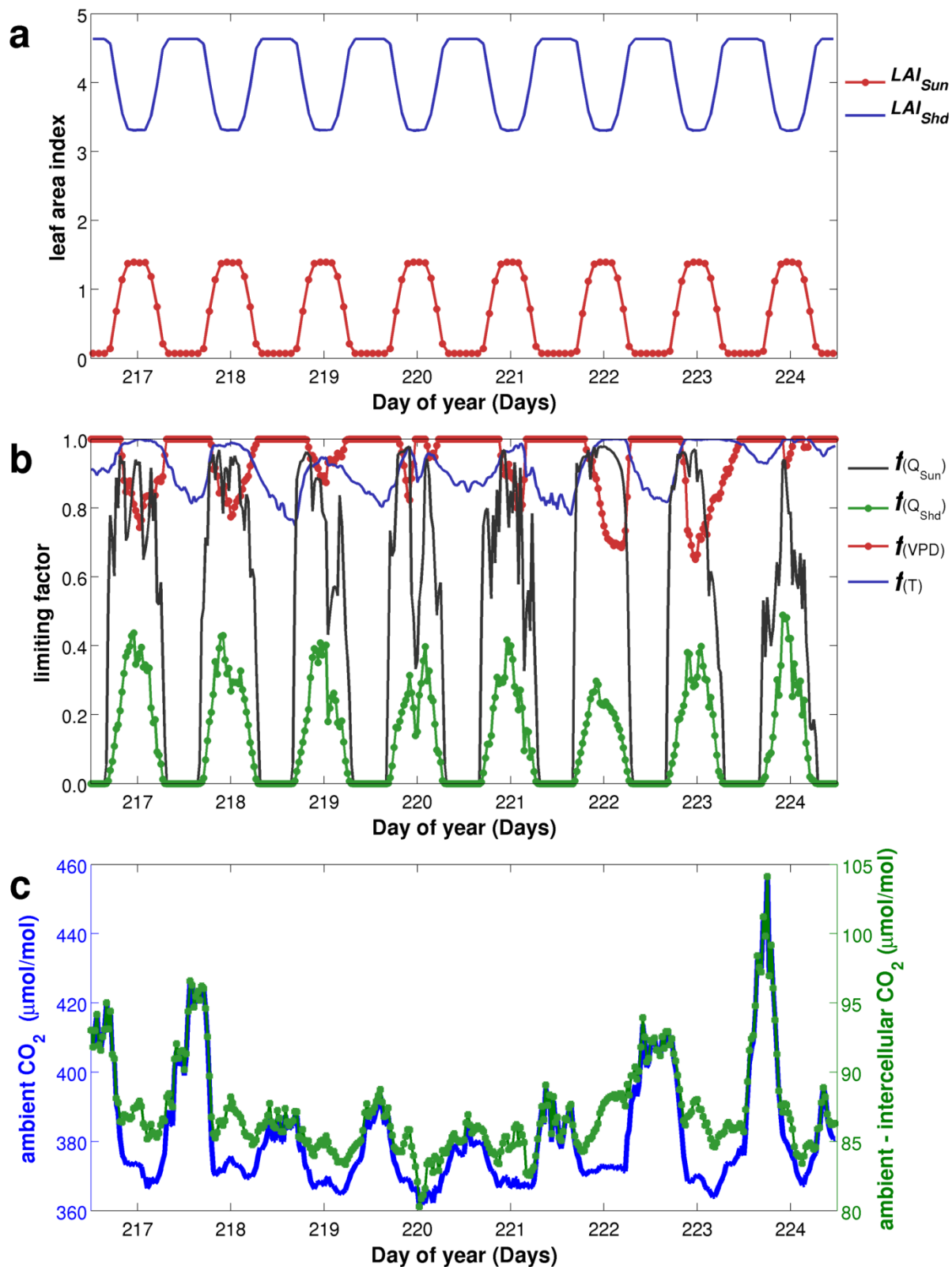
407

408 ~~Figure 4: Time series of measured and modeled components of a) the partition of global solar radiation and~~
 409 ~~b) surface radiation balance are shown for 8 successive days. Measured and modeled components of~~
 410 ~~radiation in 8 successive days are shown for a) the partition of global solar radiation, b) surface radiation~~

411 | balance, c) modeled and measured diffuse radiation, and d) modeled and measured net radiation.
412 Extraterrestrial radiation is derived following methods outlined in Allen et al. (1998). Muneer's method is
413 applied to model diffuse radiation. The GORT model is applied to model net radiation. Data are shown from
414 the Day of Year 217 to 224 in 2004 for the US-Bar site.
415

416 Time series of each component for modeling canopy photosynthesis are shown in Figure 5. Given that total
417 LAI remains the same over the course of several days, modeled sunlit and shaded LAI have little day-to-day
418 variability and only vary as a function of solar zenith angle (Figure 5a). As solar zenith angle decreases,
419 sunlit LAI increases but shaded LAI decreases. Because sunlit leaves receive more illumination, they have
420 less radiation limitations on photosynthesis than shaded leaves (Figure 5b). Temperature limitation generally
421 decreases from morning until noon, while VPD limitation increases. Although the chemical process of
422 photosynthesis favors higher temperatures, leaf stomata tend to close to reduce water loss when atmospheric
423 dryness is high (Bonan, 2002). Because short-term canopy CO₂ concentrations vary with winds and
424 convection between the ecosystem and the atmosphere, the ambient CO₂ concentrations exhibit the greatest
425 variation from day to day (Figure 5b), so do the modeled differences between ambient and intercellular CO₂
426 concentrations.

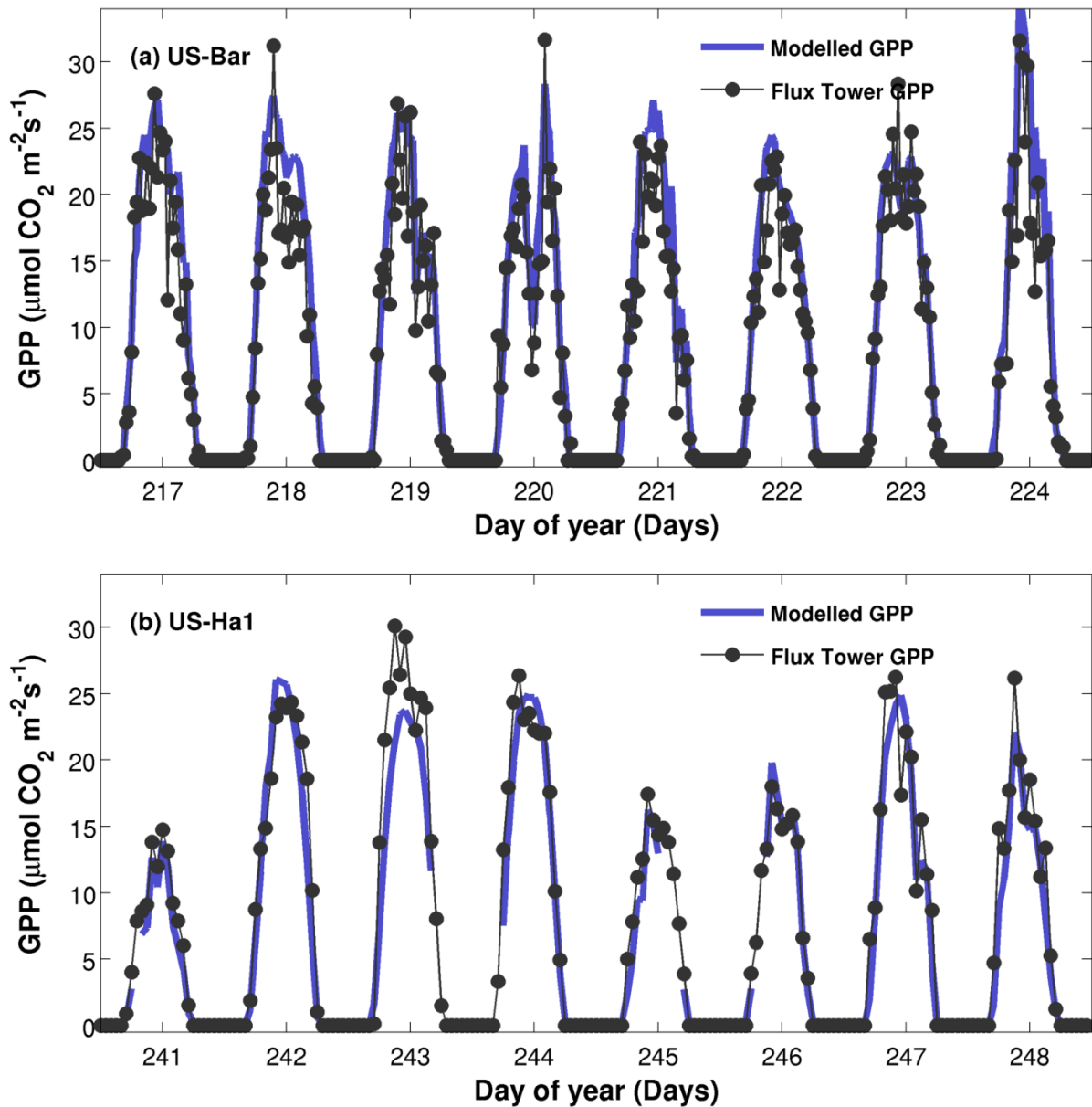
427



428

429 Figure 5: Time series of components of the photosynthesis calculation shown for a) sunlit and shaded leaf
 430 area index, b) environmental limiting factors imposed by radiation absorption, temperature, and vapor
 431 pressure deficit, and c) CO₂ concentration. Data are shown from the Day of Year 217 to 224 in 2004 for the
 432 US-Bar site.
 433

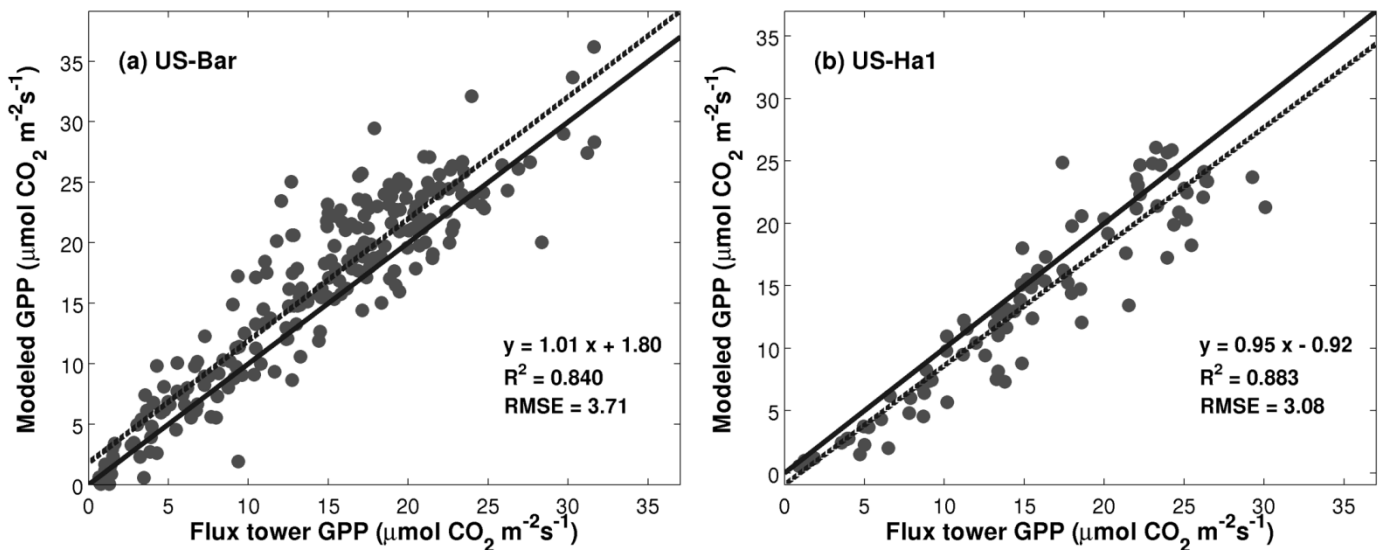
434 Figure 6 shows time series of measured and modeled GPP for two sites over eight successive days. GPP
435 estimates match flux tower measurements well in terms of the phase and amplitude. Daily peak GPP from
436 tower measurements are over $30.0 \mu\text{mol CO}_2 \text{ m}^{-2} \text{ s}^{-1}$ for both sites. It is also evident that modeled results can
437 capture some subtle variations in GPP at the hourly time scale. However, GPP estimates are slightly higher
438 on DOY 242 but lower on DOY 243 for US-Ha1. Note that we used Muneer's method for estimating the
439 diffuse radiation in US-Ha1 because measurements were not available. Considering uncertainties from the
440 partition of global solar radiation, results for both sites perform well in general.



441

442 Figure 6: Time series of modeled and measured GPP for 8 consecutive days at the sites (a) US-Bar and (b)
 443 US-Ha1. Data are half-hourly at the US-Bar site and hourly at the US-Ha1 site. Data are shown from DOY
 444 217 to 224 in 2004 for US-Bar, and from DOY 241 to 224 in 2006 for US-Ha1. Negative GPP
 445 measurements are set to zero. Missing points in modeled GPP at the US-Ha1 site are due to missing
 446 measurement of canopy CO₂ concentrations or other meteorological variables.
 447

448 Figure 7 statistically compares measured and modeled GPP. Our model is able to explain 84.0% and 88.3%
 449 of the GPP variances for the US-Bar and US-Ha1 sites, respectively. The regression lines are close to the 1 :
 450 1 lines, and GPP is only slightly overestimated for US-Bar and underestimated for US-Ha1. The root mean
 451 squared errors (RMSE) are 3.71 and 3.08 $\mu\text{mol CO}_2 \text{ m}^{-2} \text{ s}^{-1}$ for US-Bar and US-Ha1, respectively. The
 452 overall model performance is high considering that we did not attempt to perform model calibrations.
 453



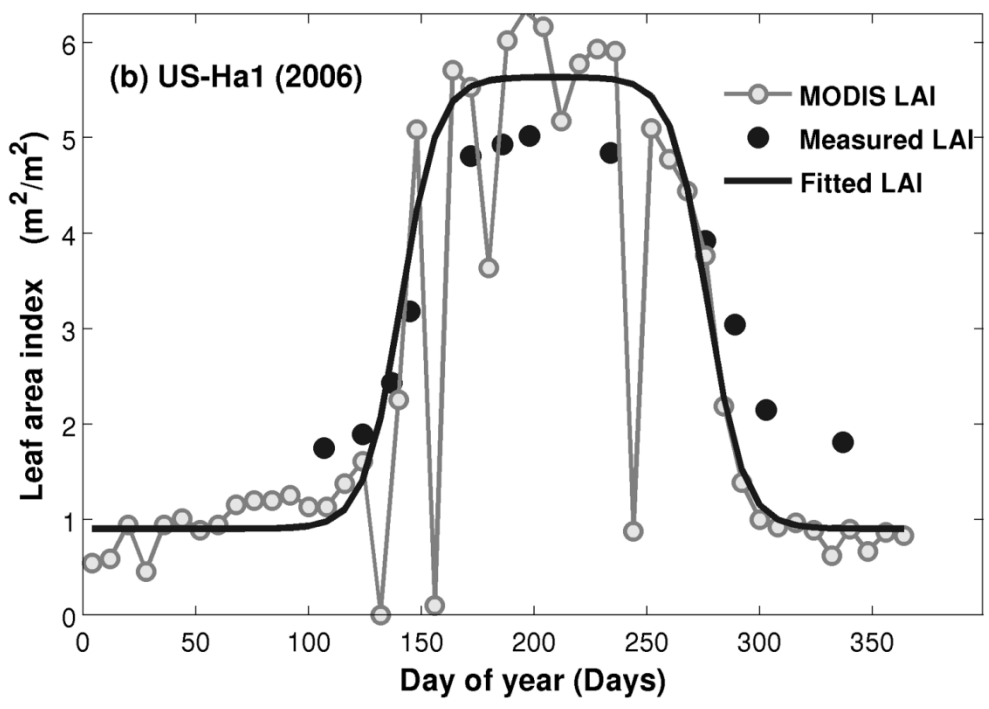
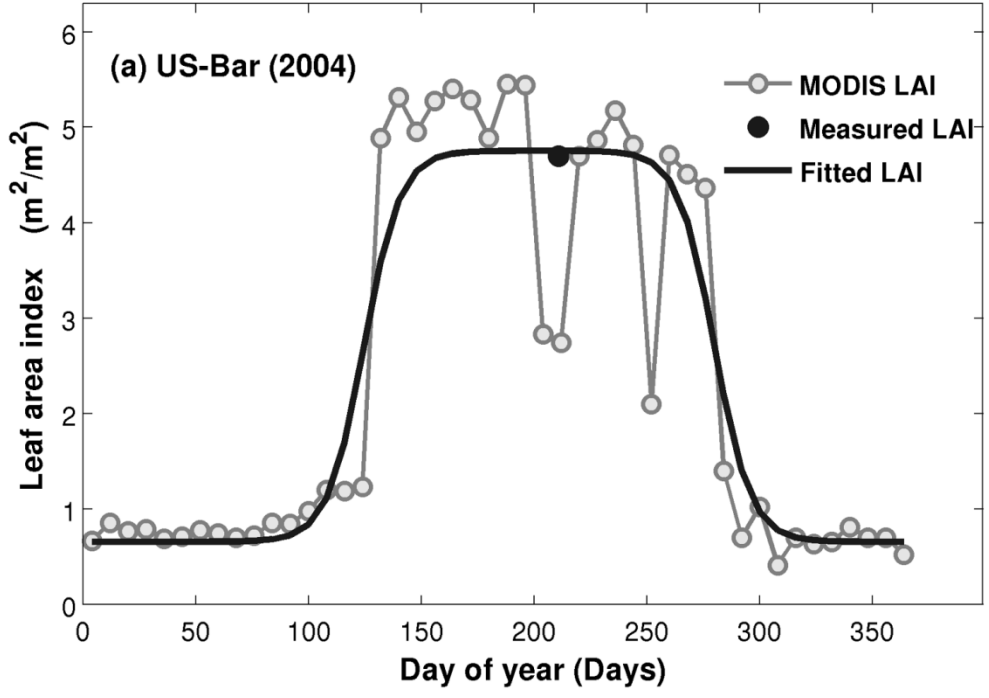
455 Figure 7: Regressions between modeled and measured GPP for 8 consecutive days at the sites (a) US-Bar
 456 and (b) US-Ha1. Data are from DOY 217 – 224 in 2004 for US-Bar and from DOY 241 to 224 in 2006 for
 457 US-Ha1. Only data during the photosynthetically active period (flux tower GPP > 0.5 $\mu\text{mol CO}_2 \text{ m}^{-2} \text{ s}^{-1}$) are
 458 included in the regression. The solid lines denote the 1 : 1 lines, and the dashed lines denote the regression
 459 lines.
 460

461 4.3 Model simulation over entire years

462 LAI derived from satellite observations (Figure 8) are used as inputs to model daily GPP over an entire year
 463 in addition to the 8-day model simulations. The double logistic fitting lines are shown to reduce noises in
 464 time series of MODIS LAI due to the effects of clouds and solar and viewing geometry. Fitted LAI time

465 series are slightly higher from June to August and lower from September to December in 2006 at the US-
466 Ha1 sites, but match with field measurements in general. The differences are likely to be introduced by
467 mismatched observation footprints and uncertainties in satellite retrieval algorithms. The fitted time series of
468 MODIS LAI are used for subsequent model simulations.

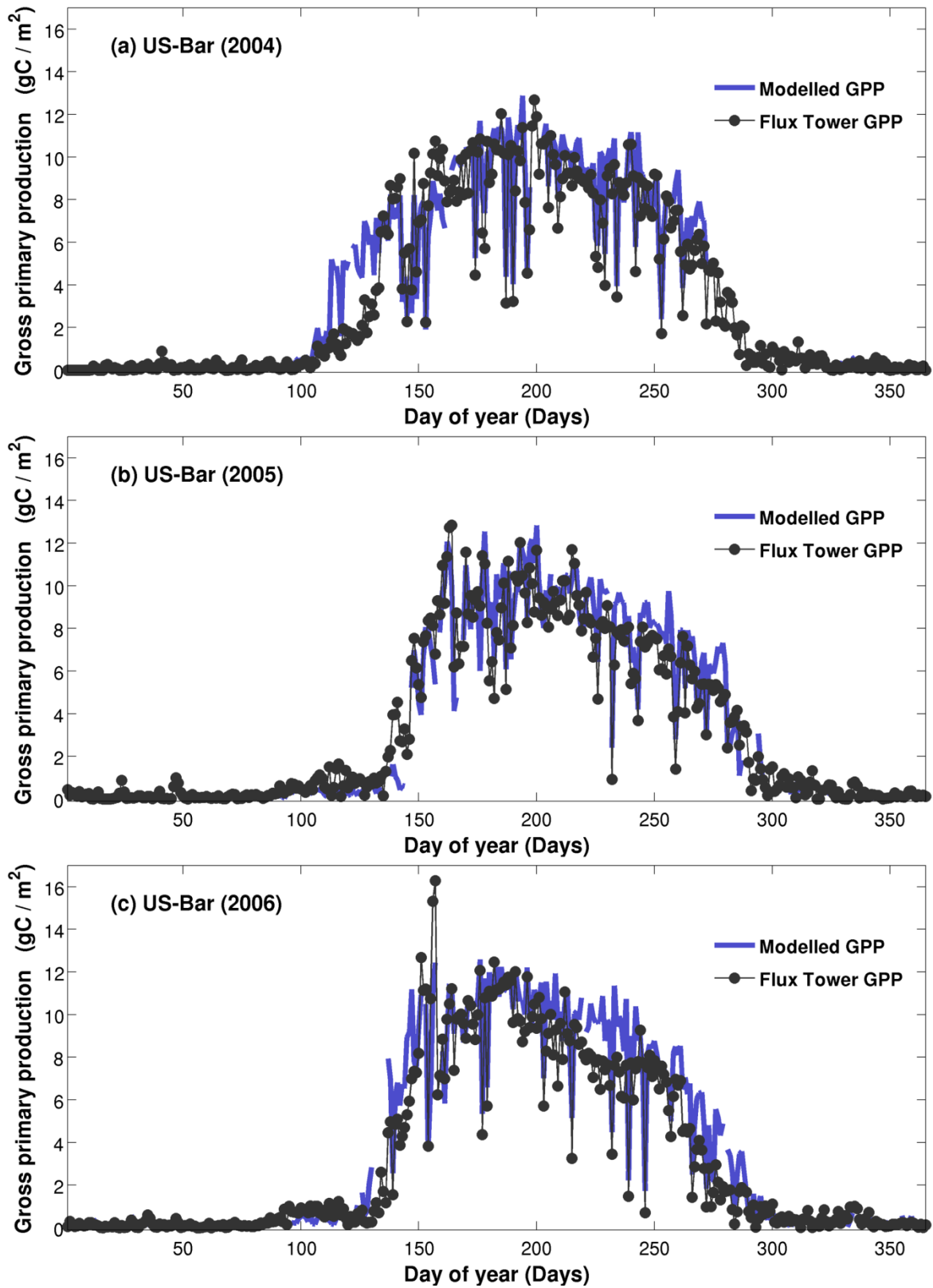
469



470

471 Figure 8: Comparisons of field-measured and satellite-derived leaf area indexes (LAI) for the sites a) US-
472 Bar in 2004 and b) US-Ha1 in 2006. The solid grey lines denote MODIS LAI as obtained from standard
473 MODIS FPAR/LAI products (MOD15A2). The solid black lines denote double logistic fitting lines that are
474 applied to MODIS LAI. The solid points denote the measured LAI as obtained from biological datasets
475 from AmeriFlux website.
476

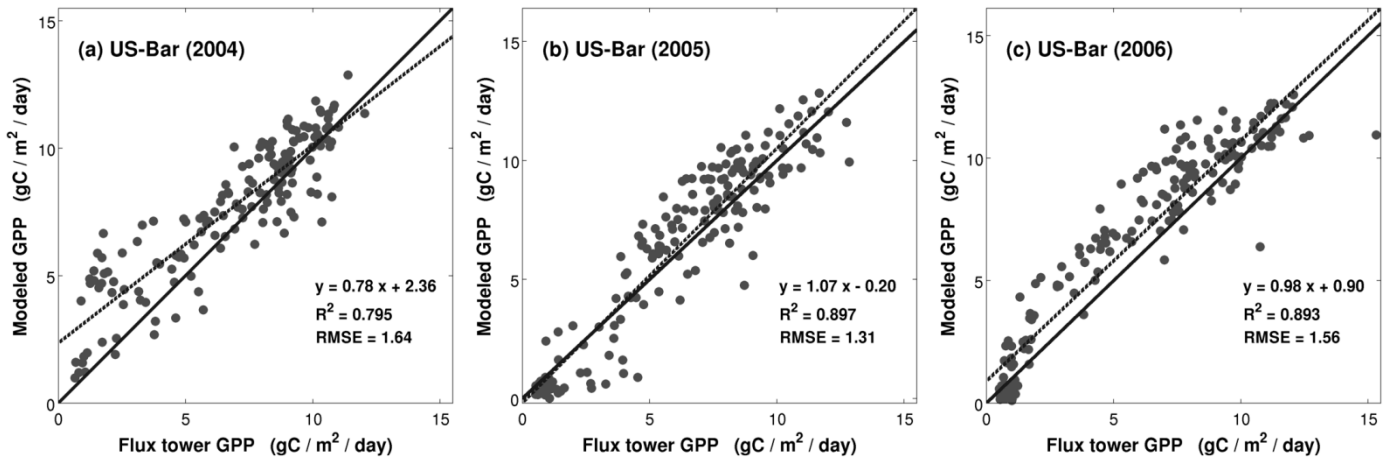
477 Figure 9 presents time series of measured and modeled GPP at the US-Bar site. Modeled results capture the
478 trend and subtle variations of measured GPP on a daily basis. Most of the dips in the GPP time series occur
479 on cloudy days when radiation is the main limiting factor for vegetation photosynthesis. GPP values at US-
480 Bar are slightly overestimated from DOY 100 to 150 in 2004 possibly due to overestimation of the LAI.
481 Statistically, modeled results can explain 79.5%, 89.7%, and 89.3% of the variance in daily GPP for the
482 years 2004, 2005, and 2006, respectively (Figure 10). Regression slopes are close to the 1 : 1 lines except in
483 the year 2004 due to overestimated GPP in the early growing season. The RMSEs are 1.64, 1.31, and 1.56
484 $\text{gC m}^{-2} \text{ day}^{-1}$ for 2004, 2005, and 2006, respectively.



485

486 Figure 9: Time series of modeled and measured daily GPP shown for (a) 2004, (b) 2005, and (c) 2006 at the
 487 US-Bar site. Model simulation is performed at a half-hourly time step. Measured and modeled half-hourly
 488 GPP are aggregated to generate daily time series with units converted from $\mu\text{mol CO}_2 \text{ m}^{-2} \text{ s}^{-1}$ to $\text{gC m}^{-2} \text{ day}^{-1}$.
 489 Occasional negative GPP measurements are set to zeros. Missing points in modeled GPP time series are

490 due to missing measurements of meteorological variables during the daytime photosynthetically active
491 period (flux tower GPP > 0.5 $\mu\text{mol CO}_2 \text{ m}^{-2} \text{ s}^{-1}$).
492



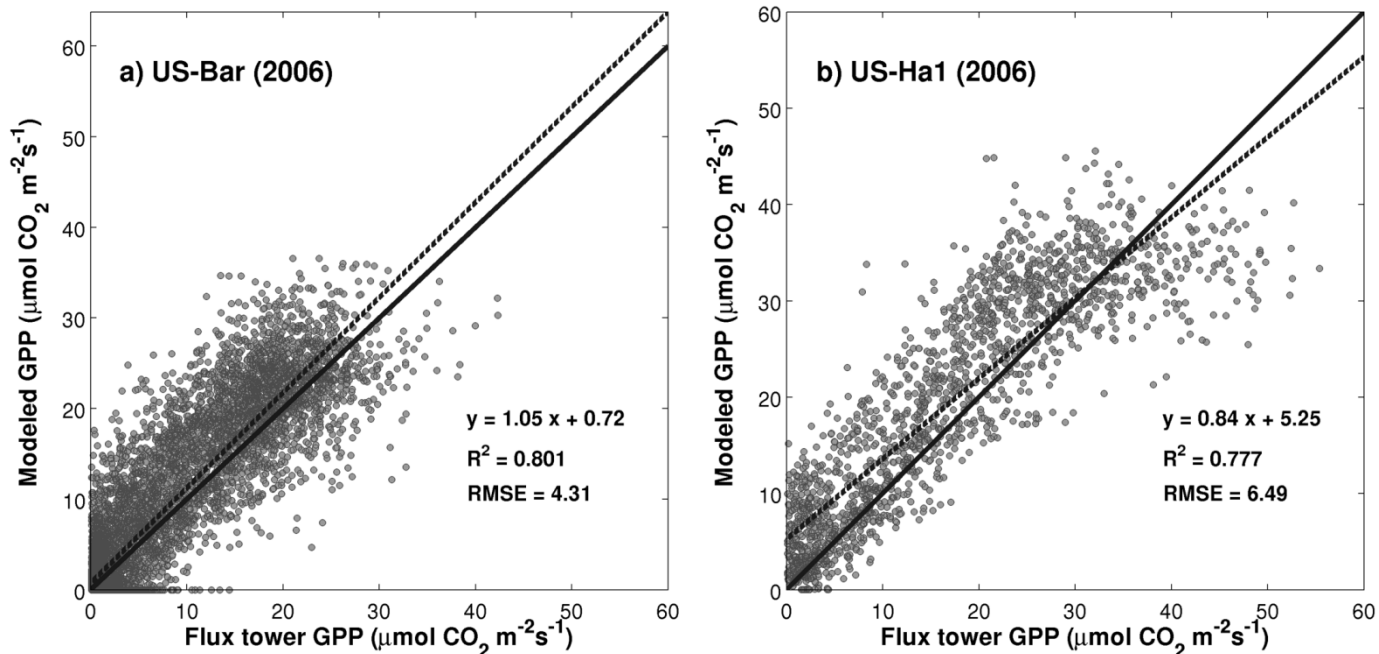
493

494 Figure 10: Regressions between modeled and measured daily GPP shown for (a) 2004, (b) 2005, and (c)
495 2006 at the US-Bar site. Only data during the photosynthetically active period (flux tower GPP > 0.5 gC m^{-2}
496 day^{-1}) are included in the regressions. The solid line denote the 1 : 1 lines, and the dashed lines denote the
497 regression lines.
498

499

499 Because measurements of atmospheric CO_2 concentrations within the canopy are largely unavailable for
500 US-Ha1 (only approximately 41.4% of the measurements are valid for use), we do not aggregate hourly
501 results to daily sums but perform regression analysis using all available hourly data in Figure 11. For the
502 US-Bar site, the R^2 value is 0.801 and the RMSE value is $4.31 \mu\text{mol CO}_2 \text{ m}^{-2} \text{ s}^{-1}$. For the US-Ha1 site,
503 Correlations—the correlation between modeled and measured GPP are-is strong with an R^2 value of 0.777 and
504 an RMSE value of $6.49 \mu\text{mol CO}_2 \text{ m}^{-2} \text{ s}^{-1}$. There were slight GPP underestimates when measured GPP
505 values are high at the US-Ha1 site, possibly due to empirical functions that we used in modeling diffuse
506 radiation and leaf photosynthesis. Table 3 lists major statistical results for our model performance, as
507 evaluated using all available hourly data at both sites. The model performance is consistent through time
508 and is comparable to the simulation of 8-day data (Figure 7), despite the fact that satellite-derived LAI
509 instead of field measurements were used for yearly simulation.
510

510



511

512 Figure 11: Regressions between modeled and measured GPP for all available hourly data at the [sites of a\)](#)
 513 [US-Bar and b\) US-Ha1 site](#) in 2006. Only data from the photosynthetically active period are included in the
 514 regression. The solid line denotes the 1 : 1 line, and the dashed line denotes the regression line.

515

516 [Table 3. The model performance at two study sites as evaluated using hourly data. Units for root mean](#)
 517 [square error \(RMSE\) and mean bias error \(Bias\) are in \$\mu\text{mol CO}_2 \text{ m}^{-2} \text{ s}^{-1}\$.](#)

Year	US-Bar			US-Ha1		
	R ²	RMSE	Bias	R ²	RMSE	Bias
2001				0.804	5.44	2.00
2002				0.729	6.75	3.09
2003				0.781	5.62	2.85
2004	0.784	4.28	1.01	0.737	6.39	1.85
2005	0.795	4.11	0.47	0.736	6.83	1.18
2006	0.801	4.31	1.06	0.777	6.49	2.28
2007				0.768	6.21	2.50
2008				0.689	7.34	3.10
2009				0.662	7.62	3.68
2010				0.752	6.55	0.35
2011				0.715	6.96	1.34

518

519

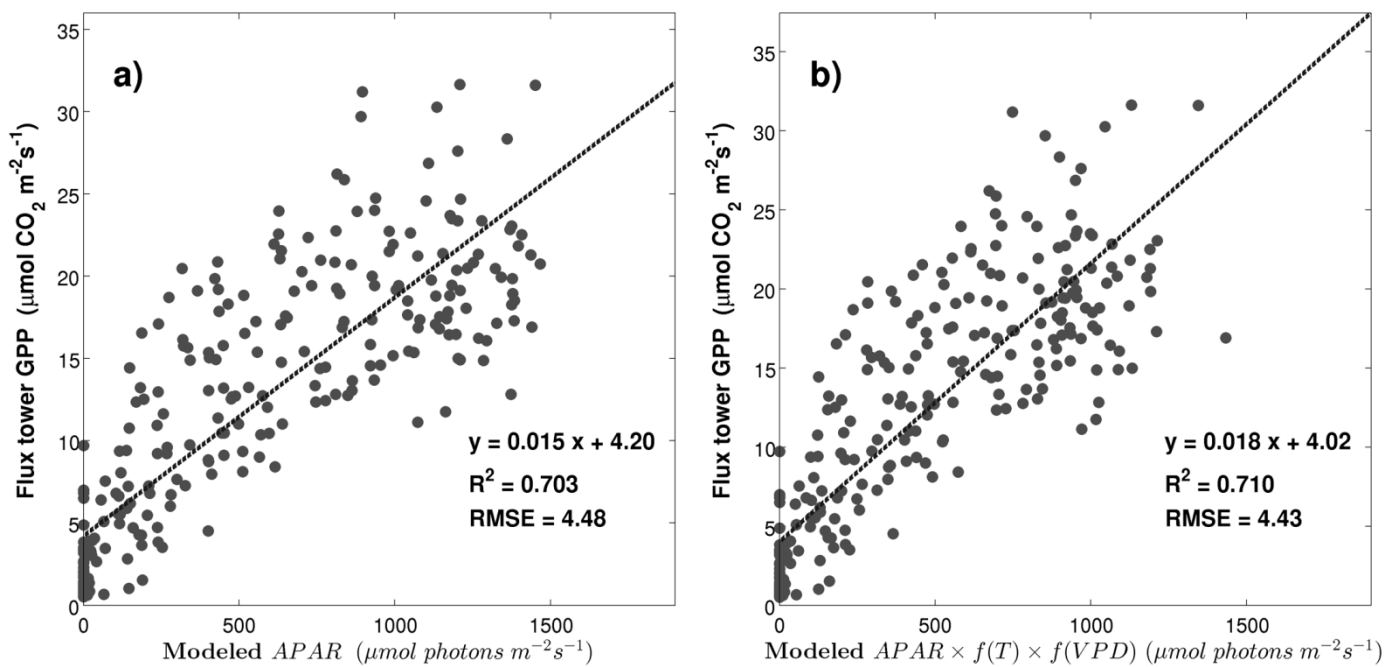
520 5. Discussion

521 5.1 Influence of CO₂ concentration on canopy photosynthesis

522 One important question is whether it is necessary to link radiative transfer with leaf stomatal conductance
 523 for modeling photosynthesis, since some ~~state-of-the-art~~ biogeochemical models such as Production

524 Efficiency Models simply assume that vegetation GPP/NPP is linearly related to canopy radiation
 525 absorption (Xin et al., 2013). To understand the performance of Production Efficiency Models, we conduct
 526 linear regressions between modeled APAR and measured GPP as shown in Figure 12. Indeed, canopy APAR
 527 is positively related to flux tower GPP and explains 70.3% of its variance. The R^2 value increases slightly to
 528 0.710 after accounting for the influences of temperature and vapor pressure. The model performance here is
 529 comparable to results from other studies that evaluate Production Efficiency Models (Chen et al., 2011;
 530 Sjöström et al., 2013; Xin et al., 2015).

531



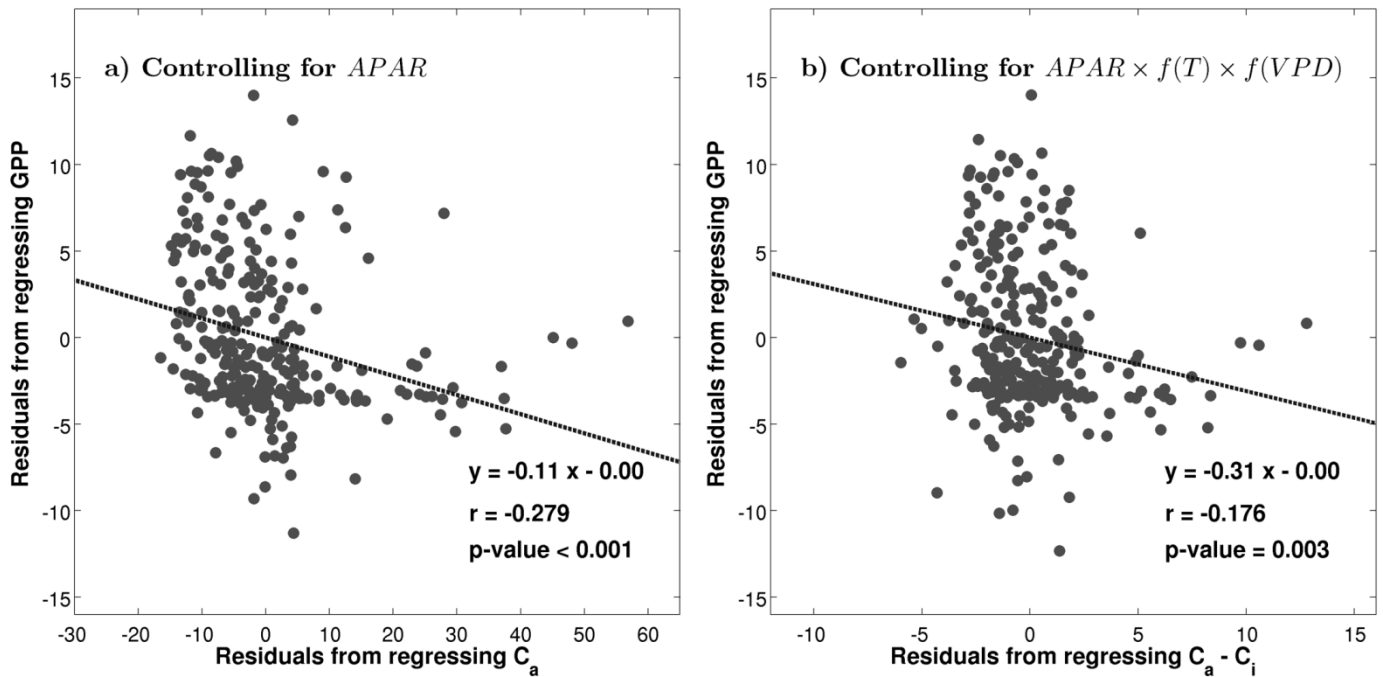
532

533 Figure 12: Regressions between modeled absorbed photosynthetic active radiation (APAR) and measured
 534 GPP. Half-hourly data are shown from DOY 217 – 224 in 2004 for US-Bar. The influences of temperature
 535 and vapor pressure deficit are modeled based on Equations (51) and (52). Only data during the
 536 photosynthetically active period are included in the regression. The dashed lines denote the regression lines.
 537

538 However, there are strong partial correlations between canopy CO_2 concentrations and GPP even after
 539 accounting for radiation absorption. Figure 13a shows the residual plot of GPP versus ambient CO_2
 540 concentrations when controlling on APAR. The slope is negative because the ambient CO_2 concentration, as
 541 regulated by vegetation photosynthesis and respiration activities, is normally high during the nighttime but

542 low during the daytime. The correlation coefficient is only -0.279, but it is statistically significant (p -value <
 543 0.001) under a one-tailed partial correlation test. The data clearly allow rejection of the null hypothesis that
 544 ambient CO₂ concentration has no effects on canopy photosynthesis. This relationship holds even after
 545 considering the factors of temperature and vapor pressure deficit (Figure 13b). We therefore conclude that
 546 accounting for the influence of ambient CO₂ concentrations is essential for modeling daytime GPP at the
 547 half-hourly time scale.

548



549

550 Figure 13: Residual plots are shown for a) the partial correction between GPP and measured-ambient CO₂
 551 concentration (C_a) while controlling for the variable of and modeled differences between ambient and
 552 intercellular CO₂ concentrations after controlling on the effects of modeled a) APAR and b) the partial
 553 correction between GPP and $C_a - C_i$ while controlling for the variable of $APAR \times f(T) \times f(VPD)$.

554

555 5.2 Clumping effects in the GORT model

556 The clumping effects of leaves modeled using GORT influence canopy radiative transfer processes and are
 557 worthy of further examination. Chen et al. (1997) demonstrated that the net effects of leaf clumping could
 558 be modeled by introducing a clumping index. We derive the clumping index by inverting their functions
 559 (Zhao et al., 2011) as follows:

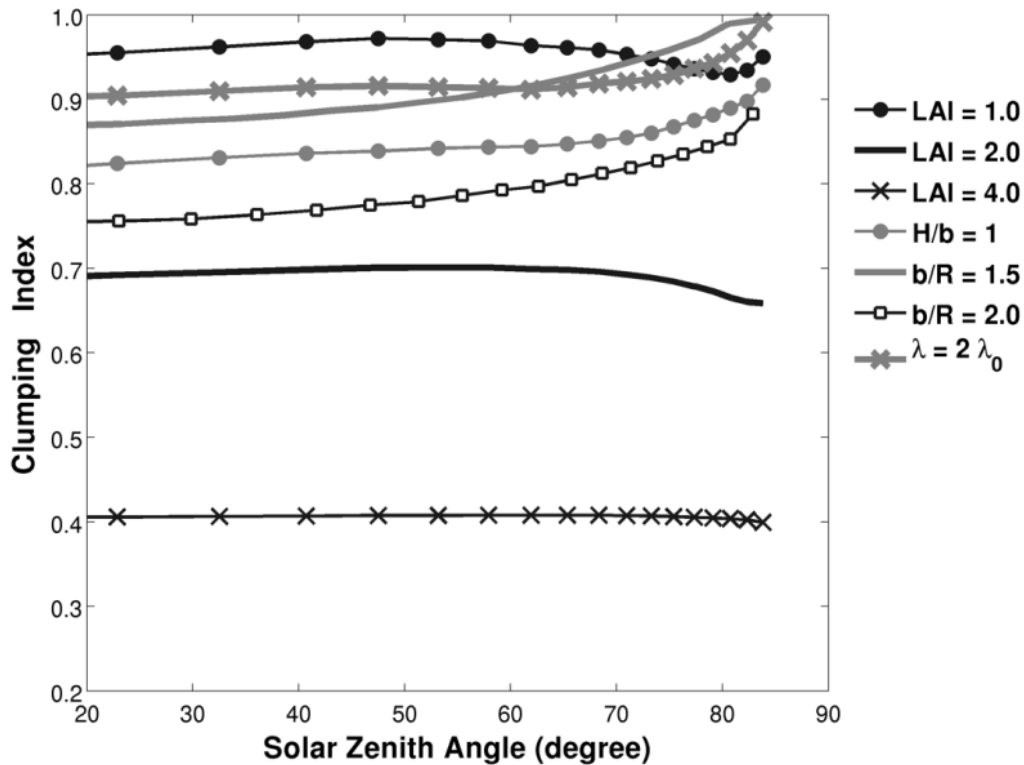
$$\Omega = \ln(P_{\text{gap}}) / \ln(P_{\text{Beer}}) = -\ln(P_{\text{gap}}) / k_b LAI \quad (58)$$

560 where Ω is the clumping index, P_{gap} is the gap probability modeled using GORT, $P_{\text{Beer}} = \exp(-k_b LAI)$ is
561 the gap probability modeled using Beer's Law, k_b is the extinction coefficient, and LAI is the leaf area
562 index.

563

564 The behavior of the derived clumping index shown in Figure 14 is intuitively interpretable. Leaves are more
565 clumped when LAI is larger given constant tree structures. However, when LAI is constant but tree density
566 increases, leaves are distributed in a larger three-dimensional space, resulting in an increased clumping
567 index. Similarly, if the H/b ratio or b/R ratio decreases while other parameters are unchanged, the total
568 crown volume increases and leaves are less clumped. The sensitivity of the clumping index to the
569 illumination zenith angle varies when using different parameter sets. Our simulated results are in line with
570 the measured and modeled results in previous studies (Leblanc and Chen, 2001; Leblanc et al., 2002): the
571 clumping indexes are insensitive to zenith angles in some forest stands and increase with zenith angles in
572 others. We do not attempt to derive clumping indexes at solar zenith angle greater than 85° when gap
573 fractions typically approach zeros. These results ~~have important biogeochemical implications: imply that~~ tree
574 structure strongly influences radiation absorption and photosynthesis of canopies. ~~In areas where canopy~~
575 ~~crowns should be treated as discrete objects, more sunlight can reach the understory and ground surface, and~~
576 ~~vegetation GPP may not be as large as that in continuous forests even if the LAIs are the same.~~

577



578

579 Figure 14: Derived clumping index as a function of solar zenith angle for varied canopy parameters. Tree
 580 parameters for US-Bar are used for GORT simulations. The default simulation is for a canopy composed of
 581 $H/b = 2.0$, $b/R = 3.0$, $\lambda = 1432$ trees/ha, and $LAI = 2.0$, and labeled curves are for the same case with
 582 only the labeled parameters varied.

583

584 5.3 Assumptions and future improvements

585 It is also necessary to review our model assumptions and identify possible avenues for future improvements.

586 First, we assume a spherical leaf angle distribution in the model simulations. However, most deciduous

587 forests have semi-horizontal leaf orientation (Bonan, 2002) and an assumption of planophile or plagiophile

588 LAD is likely to be more appropriate for temperate and boreal broadleaf forests (Pisek et al., 2013). Because

589 LAD influences the proportions of sunlit and shaded leaf areas, the way in which modeled canopy GPP

590 varies with LAD requires further exploration. Second, the substrate under the canopy layer is assumed to be

591 a Lambertian surface. Field studies have observed the effects of bi-directional reflectance distribution

592 function (BRDF) for soils (Liang and Townshend, 1996; Wang et al., 2010), and coupled soil and vegetation

593 model (Ni and Li, 2000; Verhoef and Bach, 2007) should be tested to understand the effects of soil BRDF

594 on canopy photosynthesis. Third, we assume maximum constant leaf stomatal conductance over the

595 growing season. It is worth examining how optimal leaf stomatal conductance may evolve with leaf
596 development stages and long-term environmental changes (Keenan et al., 2013; Lammertsma et al., 2011).
597 Fourth, we use ellipsoids to describe tree crown shapes for deciduous broadleaf forests. Because many
598 evergreen needleleaf forests have conical crowns, future applications to areas with conifer forests may
599 require different treatment on crown shapes in the models. Finally, our linkage between radiative transfer
600 and biochemical processes is still empirical. We may need to test other mechanisms, for example, the
601 biochemical model based on the enzyme kinetics of rubisco and the regeneration of RuBP in response to
602 light absorption (Farquhar and Sharkey, 1982), in future studies.

603

604 **6. Conclusion**

605 We propose and validate a new model that links GORT with biochemical processes for modeling canopy
606 photosynthesis. Several main conclusions can be drawn from this study. First, the radiative transfer process
607 within the canopy is one of the key factors in modeling vegetation photosynthesis, and our proposed model
608 simulates canopy photosynthesis well. Modeled GPP robustly explained approximately 80% or more
609 variance in GPP measurements at both half-hourly and daily time scales. Second, tree structures influence
610 canopy gap probabilities and vegetation photosynthesis. Leaf clumping could vary as a function of tree
611 density, canopy depth, and crown shapes and affect canopy sunlight interception. ~~Finally, ambient CO₂~~
612 ~~concentration controls vegetation photosynthesis activities and should be included in state-of-the-art~~
613 ~~biogeochemical models.~~ Finally, ambient CO₂ concentrations influence vegetation photosynthesis activities
614 and should be included in biogeochemical models.

615

616 Accurate modeling of vegetation photosynthesis is essential for improving our understanding of the global
617 carbon cycle. The model we developed is complementary to classic radiative transfer models, especially in
618 sparse and intermediate forest stands. Although more validation efforts are required, the GORT-
619 photosynthesis model is promising in terms of simulating photosynthesis for discontinuous plant canopies.

621 **Appendix A:**

622 Table A1. Nomenclature

Symbols	Definition
$P_{\text{gap}}(h, \theta_i)$	total gap probability for beam light passing through the canopy
$P_{\text{gap}}(n = 0 h, \theta_i)$	gap probability for beam light passing through the canopy without reaching any crowns
$P_{\text{gap}}(n > 0 h, \theta_i)$	gap probability for beam light passing through crowns without being intercepted by leaves
$P(s h, \theta_i)$	probability distribution function associated with within-crown path length
$P(s n, z, h, \theta_i)$	probability distribution of within-crown path length given that a solar ray enters the crown at height h and angle θ_i
$P(n z, h, \theta_i)$	probability distribution of the numbers of crowns intercepted by the solar ray incident at angle θ_i , entering crowns at height z , and then traveling to height h
λ_v	tree density (m^{-2})
V_Γ	projected cylinder volume starting from the canopy top and extending to certain height
$\tau(\theta_i, \alpha)$	projected foliage area volume density (m^{-1})
$k_b(\theta_i, \alpha)$	extinction coefficient for beam radiation
k_d	extinction coefficient for diffuse radiation
$K_{\text{open}}(h)$	canopy openness factor to diffuse radiation
$K_{\text{open}}(n = 0 h)$	between-crown openness factor
$K_{\text{open}}(n > 0 h)$	within-crown openness factor
$P'_{\text{gap}}(h, \theta_i)$	the first derivative of gap probability $P_{\text{gap}}(h, \theta_i)$ with respect to height
$K'_{\text{open}}(h)$	the first derivative of the openness factor $K_{\text{open}}(h)$ with respect to height
$t_0(h, \theta_i)$	the proportion of unintercepted direct beam for semi-infinite homogeneous canopies
R_{ff}^∞	hemispherical-hemispherical reflectance for semi-infinite homogeneous canopies
R_{df}^∞	directional-hemispherical reflectance for semi-infinite homogeneous canopies
T_{ff}^∞	hemispherical-hemispherical transmittance for semi-infinite homogeneous canopies
T_{df}^∞	directional-hemispherical transmittance for semi-infinite homogeneous canopies
$\rho_{ff}(h)$	hemispherical-hemispherical reflectance for homogeneous canopies with finite thickness
$\rho_{df}(h, \theta_i)$	directional-hemispherical reflectance for homogeneous canopies with finite thickness
$t_{ff}(h)$	hemispherical-hemispherical transmittance for homogeneous canopies with finite thickness
$t_{df}(h, \theta_i)$	directional-hemispherical transmittance for homogeneous canopies with finite thickness
$\rho'_{ff}(h)$	hemispherical-hemispherical reflectance for discontinuous canopies
$\rho'_{df}(h, \theta_i)$	directional-hemispherical reflectance for discontinuous canopies
$t'_{ff}(h)$	hemispherical-hemispherical transmittance for discontinuous canopies
$t'_{df}(h, \theta_i)$	directional-hemispherical transmittance for discontinuous canopies
$\delta LAI(h)$	leaf area index within a thin layer δh at height h
LAI	total leaf area index of the canopy
$LAI_{\text{Sun}}(\theta_i)$	sunlit leaf area index given a solar illumination angle θ_i
$LAI_{\text{Shd}}(\theta_i)$	shaded leaf area index given a solar illumination angle θ_i
$LAI_{\text{Sun}}^*(\theta_i)$	sunlit leaf area for homogeneous canopies given a solar illumination angle θ_i
θ_i	solar illumination angle
ϕ	azimuth angle
σ	leaf single scattering albedo
γ	$\sqrt{1 - \sigma}$
μ_i	$\cos(\theta_i)$
ρ_l	leaf reflectance
τ_l	leaf transmittance
ρ_s	soil reflectance

ρ_{cb}	canopy reflection coefficient for beam irradiance
ρ_{cd}	canopy reflection coefficient for diffuse irradiance
f_b	the fraction of incident beam radiation in total or global incoming solar radiation
$I_b(h, \theta_i)$	unintercepted beam fluxes at canopy height h given a solar illumination angle θ_i
$I_d(h)$	unintercepted diffuse fluxes at canopy height h
$I_{bt}(h, \theta_i)$	unintercepted and down scattered beam fluxes
$I_{dt}(h)$	unintercepted and down scattered diffuse fluxes
I_c	total radiation absorbed by canopy elements
I_{cb}	beam radiation absorbed by canopy elements
I_{cd}	diffuse radiation absorbed by canopy elements
I_{Sun}	total radiation absorbed by sunlit leaves
I_{Sunb}	beam radiation directly absorbed by sunlit leaves
I_{Sunbs}	down scattered beam radiation absorbed by sunlit leaves
I_{Sund}	diffuse radiation absorbed by sunlit leaves
I_{Sun}	total radiation absorbed by shaded leaves
Q_{Sun}	total radiation absorbed by sunlit leaves per leaf hemi-surface area
Q_{Shd}	total radiation absorbed by shaded leaves per leaf hemi-surface area
A	leaf-level CO ₂ assimilation rate
g_c	stomatal conductance
C_a	ambient CO ₂ concentrations
C_i	intercellular CO ₂ concentrations
g_{cSun}	stomatal conductance for sunlit leaves
g_{cShd}	stomatal conductance for shaded leaves
g_{cmax}	maximum leaf stomatal conductance when environmental factors do not limit carbon uptake
$f(x_i)$	scalars that account for the influences of environmental stresses on leaf stomatal conductance
$f(Q)$	scalars that account for the influences of solar radiation on leaf stomatal conductance
$f(T)$	scalars that account for the influences of temperature on leaf stomatal conductance
$f(VPD)$	scalars that account for the influences of vapor pressure deficit on leaf stomatal conductance
k_C	stress coefficients of PAR absorbed by plant leaves for the temperature scalar
k_Q	stress coefficients of PAR absorbed by plant leaves for the temperature scalar
T_{min}	minimum temperature for photosynthetic activities
T_{max}	maximum temperature for photosynthetic activities
T_{opt}	optimum temperature for photosynthetic activities
VPD	ambient vapor pressure deficit
VPD_{min}	minimum vapor pressure deficit
VPD_{max}	maximum vapor pressure deficit
VPD_0	an empirical constant describing the species sensitivity to ambient vapor pressure deficit
Γ	leaf CO ₂ compensation point
m_L	regression coefficient for ambient and intercellular CO ₂ concentrations related to tree species
A_{Sun}	leaf-level CO ₂ assimilation rate for sunlit leaves
A_{Shd}	leaf-level CO ₂ assimilation rate for shaded leaves
K_t	hourly clearness index
I_0	total or global incoming solar radiation on a horizontal plane at the canopy top
I_e	extraterrestrial solar radiation
Ω	foliage clumping index
P_{Beer}	gap probability for beam light passing through the canopy as modeled using Beer's Law

623

624 | Table A2. Values for model parameters

<u>Symbols</u>	<u>Value</u>	<u>Units</u>	<u>Reference</u>
k_C	500	W / m ²	Ding et al. (2014)
k_Q	150	W / m ²	Ding et al. (2014)

T_{min}	<u>0</u>	<u>°C</u>	<u>Kalfas et al. (2011)</u>
T_{max}	<u>45</u>	<u>°C</u>	<u>Kalfas et al. (2011)</u>
T_{opt}	<u>25</u>	<u>°C</u>	<u>Kalfas et al. (2011)</u>
VPD_{min}	<u>0.65</u>	<u>kPa</u>	<u>Heinsch et al. (2003)</u>
VPD_{max}	<u>4.6</u>	<u>kPa</u>	<u>Heinsch et al. (2003)</u>
VPD_0	<u>30</u>	<u>kPa</u>	<u>Katul et al. (2000)</u>
Γ	<u>40</u>	<u>$\mu\text{mol/mol}$</u>	<u>Katul et al. (2000)</u>
m_L	<u>4.0</u>		<u>Katul et al. (2000)</u>

625

626 **Author contribution**

627 Qinchuan Xin developed the model code and performed the simulations. Qinchuan Xin designed the
628 experiments and Wenyu Li contributed to data analysis. Qinchuan Xin and Peng Gong prepared the
629 manuscript with contributions from all co-authors.

630

631 **Acknowledgments**

632 We gratefully thank Alan H. Strahler, Xiaowen Li, Crystal B. Schaaf, Curtis E. Woodcock, and Wenge Ni-
633 Meister for their contributions to the development of the original GORT model. We thank the researchers
634 and investigators involved in data collection and analysis at the AmeriFlux sites. This research was
635 supported by the National Natural Science Foundation of China (Grant no. 41401484 [and 51209220](#)). We
636 also thank anonymous reviewers for their constructive comments.

637

638 **References**

639 Allen, R. G., Pereira, L. S., Raes, D., and Smith, M.: Crop evapotranspiration-Guidelines for computing
640 crop water requirements-FAO Irrigation and drainage paper 56, FAO, Rome, 300, 6541, 1998.

641 Baldocchi, D., Falge, E., Gu, L., Olson, R., Hollinger, D., Running, S., Anthoni, P., Bernhofer, C., Davis, K.,
642 and Evans, R.: FLUXNET: A new tool to study the temporal and spatial variability of ecosystem-scale
643 carbon dioxide, water vapor, and energy flux densities, *Bulletin of the American Meteorological Society*, 82,
644 2415-2434, 2001.

645 Baldocchi, D., Hutchison, B., Matt, D., and McMillen, R.: Canopy radiative transfer models for spherical
646 and known leaf inclination angle distributions: a test in an oak-hickory forest, *Journal of Applied Ecology*,
647 1985. 539-555, 1985.

- 648 Baldocchi, D. D.: Assessing the eddy covariance technique for evaluating carbon dioxide exchange rates of
649 ecosystems: past, present and future, *Global Change Biology*, 9, 479-492, 2003.
- 650 Ball, J. T., Woodrow, I., and Berry, J.: A Model Predicting Stomatal Conductance and its Contribution to the
651 Control of Photosynthesis under Different Environmental Conditions. In: *Progress in Photosynthesis*
652 *Research*, Biggins, J. (Ed.), Springer Netherlands, 1987.
- 653 Bonan, G. B.: *Ecological climatology: concepts and applications*, Cambridge University Press, 2002.
- 654 Bonan, G. B.: Forests and climate change: forcings, feedbacks, and the climate benefits of forests, *science*,
655 320, 1444-1449, 2008.
- 656 Broich, M., Huete, A., Tulbure, M. G., Ma, X., Xin, Q., Paget, M., Restrepo-Coupe, N., Davies, K.,
657 Devadas, R., and Held, A.: Land surface phenological response to decadal climate variability across
658 Australia using satellite remote sensing, *Biogeosciences*, 11, 5181-5198, 2014.
- 659 Campbell, G. S. and Norman, J. M.: *An introduction to environmental biophysics*, Springer, 1998.
- 660 Chen, J. M., Rich, P. M., Gower, S. T., Norman, J. M., and Plummer, S.: Leaf area index of boreal forests:
661 Theory, techniques, and measurements, *Journal of Geophysical Research: Atmospheres* (1984–2012), 102,
662 29429-29443, 1997.
- 663 Chen, T., van der Werf, G. R., Dolman, A. J., and Groenendijk, M.: Evaluation of cropland maximum light
664 use efficiency using eddy flux measurements in North America and Europe, *Geophysical Research Letters*,
665 38, 2011.
- 666 Collatz, G. J., Ball, J. T., Grivet, C., and Berry, J. A.: Physiological and environmental regulation of stomatal
667 conductance, photosynthesis and transpiration: a model that includes a laminar boundary layer, *Agricultural*
668 *and Forest Meteorology*, 54, 107-136, 1991.
- 669 Cramer, W., Bondeau, A., Woodward, F. I., Prentice, I. C., Betts, R. A., Brovkin, V., Cox, P. M., Fisher, V.,
670 Foley, J. A., and Friend, A. D.: Global response of terrestrial ecosystem structure and function to CO₂ and
671 climate change: results from six dynamic global vegetation models, *Global change biology*, 7, 357-373,
672 2001.
- 673 Ding, R., Kang, S., Du, T., Hao, X., and Zhang, Y.: Scaling Up Stomatal Conductance from Leaf to Canopy
674 Using a Dual-Leaf Model for Estimating Crop Evapotranspiration, *PloS one*, 9, e95584, 2014.
- 675 Fan, W., Chen, J. M., Ju, W., and Nesbitt, N.: Hybrid Geometric Optical Radiative Transfer Model Suitable
676 for Forests on Slopes, *IEEE Transactions on Geoscience and Remote Sensing*, 52, 5579-5586, 2014.

- 677 Farquhar, G. D. and Sharkey, T. D.: Stomatal conductance and photosynthesis, Annual review of plant
678 physiology, 33, 317-345, 1982.
- 679 Field, C. B., Randerson, J. T., and Malmstrom, C. M.: Global net primary production: Combining ecology
680 and remote sensing, Remote Sensing of Environment, 51, 74-88, 1995.
- 681 Goudriaan, J.: Crop micrometeorology: a simulation study, Pudoc, Center for Agricultural Publishing and
682 Documentation, 1977.
- 683 Hapke, B.: Bidirectional reflectance spectroscopy: 1. Theory, Journal of Geophysical Research: Solid Earth
684 (1978–2012), 86, 3039-3054, 1981.
- 685 He, L., Chen, J. M., Pisek, J., Schaaf, C. B., and Strahler, A. H.: Global clumping index map derived from
686 the MODIS BRDF product, Remote Sensing of Environment, 119, 118-130, 2012.
- 687 He, M., Ju, W., Zhou, Y., Chen, J., He, H., Wang, S., Wang, H., Guan, D., Yan, J., and Li, Y.: Development
688 of a two-leaf light use efficiency model for improving the calculation of terrestrial gross primary
689 productivity, Agricultural and Forest Meteorology, 173, 28-39, 2013.
- 690 Heimann, M. and Reichstein, M.: Terrestrial ecosystem carbon dynamics and climate feedbacks, Nature,
691 451, 289-292, 2008.
- 692 Heinsch, F. A., Reeves, M., Votava, P., Kang, S., Milesi, C., Zhao, M., Glassy, J., Jolly, W. M., Loehman, R.,
693 and Bowker, C. F.: GPP and NPP (MOD17A2/A3) Products NASA MODIS Land Algorithm, MOD17
694 User's Guide, 2003. 1-57, 2003.
- 695 Jarvis, P. G. and McNaughton, K.: Stomatal control of transpiration: scaling up from leaf to region,
696 Advances in ecological research, 15, 1-49, 1986.
- 697 Kalfas, J. L., Xiao, X., Vanegas, D. X., Verma, S. B., and Suyker, A. E.: Modeling gross primary production
698 of irrigated and rain-fed maize using MODIS imagery and CO₂ flux tower data, Agricultural and Forest
699 Meteorology, 151, 1514-1528, 2011.
- 700 Katul, G., Ellsworth, D., and Lai, C. T.: Modelling assimilation and intercellular CO₂ from measured
701 conductance: a synthesis of approaches, Plant, Cell & Environment, 23, 1313-1328, 2000.
- 702 Keenan, T. F., Hollinger, D. Y., Bohrer, G., Dragoni, D., Munger, J. W., Schmid, H. P., and Richardson, A.
703 D.: Increase in forest water-use efficiency as atmospheric carbon dioxide concentrations rise, Nature, 499,
704 324-327, 2013.

- 705 Kucharik, C. J., Barford, C. C., El Maayar, M., Wofsy, S. C., Monson, R. K., and Baldocchi, D. D.: A
706 multiyear evaluation of a Dynamic Global Vegetation Model at three AmeriFlux forest sites: Vegetation
707 structure, phenology, soil temperature, and CO₂ and H₂O vapor exchange, *Ecological Modelling*, 196, 1-31,
708 2006.
- 709 Lammertsma, E. I., de Boer, H. J., Dekker, S. C., Dilcher, D. L., Lotter, A. F., and Wagner-Cremer, F.:
710 Global CO₂ rise leads to reduced maximum stomatal conductance in Florida vegetation, *Proceedings of the*
711 *National Academy of Sciences*, 108, 4035-4040, 2011.
- 712 Law, B., Falge, E., Gu, L. v., Baldocchi, D., Bakwin, P., Berbigier, P., Davis, K., Dolman, A., Falk, M., and
713 Fuentes, J.: Environmental controls over carbon dioxide and water vapor exchange of terrestrial vegetation,
714 *Agricultural and Forest Meteorology*, 113, 97-120, 2002.
- 715 Leblanc, S. G. and Chen, J. M.: A practical scheme for correcting multiple scattering effects on optical LAI
716 measurements, *Agricultural and Forest Meteorology*, 110, 125-139, 2001.
- 717 Leblanc, S. G., Chen, J. M., and Kwong, M.: Tracing radiation and architecture of canopies, *TRAC Manual*.
718 Version, 2, 25, 2002.
- 719 Leuning, R.: A critical appraisal of a combined stomatal - photosynthesis model for C₃ plants, *Plant, Cell &*
720 *Environment*, 18, 339-355, 1995.
- 721 Li, L., Friedl, M. A., Xin, Q., Gray, J., Pan, Y., and Frohling, S.: Mapping Crop Cycles in China Using
722 MODIS-EVI Time Series, *Remote Sensing*, 6, 2473-2493, 2014.
- 723 Li, X. and Strahler, A. H.: Geometric-optical bidirectional reflectance modeling of the discrete crown
724 vegetation canopy: Effect of crown shape and mutual shadowing, *IEEE Transactions on Geoscience and*
725 *Remote Sensing*, 30, 276-292, 1992.
- 726 Li, X., Strahler, A. H., and Woodcock, C. E.: A hybrid geometric optical-radiative transfer approach for
727 modeling albedo and directional reflectance of discontinuous canopies, *IEEE Transactions on Geoscience*
728 *and Remote Sensing*, 33, 466-480, 1995.
- 729 Liang, S. and Townshend, J.: A parametric soil BRDF model: A four stream approximation for multiple
730 scattering, *International journal of remote sensing*, 17, 1303-1315, 1996.
- 731 Liu, J., Woodcock, C. E., Melloh, R. A., Davis, R. E., McKenzie, C., and Painter, T. H.: Modeling the view
732 angle dependence of gap fractions in forest canopies: Implications for mapping fractional snow cover using
733 optical remote sensing, *Journal of Hydrometeorology*, 9, 1005-1019, 2008.

- 734 Monteith, J. L.: Climate and efficiency of crop production in Britain, *Philosophical Transactions of the*
735 *Royal Society of London Series B-Biological Sciences*, 281, 277-294, 1977.
- 736 Muneer, T.: *Solar radiation and daylight models*, Routledge, 2007.
- 737 Myneni, R., Maggion, S., Iaquinta, J., Privette, J., Gobron, N., Pinty, B., Kimes, D., Verstraete, M., and
738 Williams, D.: Optical remote sensing of vegetation: modeling, caveats, and algorithms, *Remote Sensing of*
739 *Environment*, 51, 169-188, 1995.
- 740 Myneni, R. B.: Modeling radiative transfer and photosynthesis in three-dimensional vegetation canopies,
741 *Agricultural and Forest Meteorology*, 55, 323-344, 1991.
- 742 Myneni, R. B., Asrar, G., and Gerstl, S. A.: Radiative transfer in three dimensional leaf canopies, *Transport*
743 *Theory and Statistical Physics*, 19, 205-250, 1990.
- 744 Myneni, R. B., Hoffman, S., Knyazikhin, Y., Privette, J. L., Glassy, J., Tian, Y., Wang, Y., Song, X., Zhang,
745 Y., Smith, G. R., Lotsch, A., Friedl, M., Morisette, J. T., Votava, P., Nemani, R. R., and Running, S. W.:
746 Global products of vegetation leaf area and fraction absorbed PAR from year one of MODIS data, *Remote*
747 *Sensing of Environment*, 83, 214-231, 2002.
- 748 Myneni, R. B., Keeling, C., Tucker, C., Asrar, G., and Nemani, R.: Increased plant growth in the northern
749 high latitudes from 1981 to 1991, *Nature*, 386, 698-702, 1997.
- 750 Ni-Meister, W., Yang, W., and Kiang, N. Y.: A clumped-foliage canopy radiative transfer model for a global
751 dynamic terrestrial ecosystem model. I: Theory, *Agricultural and forest meteorology*, 150, 881-894, 2010.
- 752 Ni, W.: *Development and application of models of the radiation regime within conifer forests*, 1998.
- 753 Ni, W. and Li, X.: A coupled vegetation–soil bidirectional reflectance model for a semiarid landscape,
754 *Remote Sensing of Environment*, 74, 113-124, 2000.
- 755 Ni, W., Li, X., Woodcock, C. E., Caetano, M. R., and Strahler, A. H.: An analytical hybrid GORT model for
756 bidirectional reflectance over discontinuous plant canopies, *IEEE Transactions on Geoscience and Remote*
757 *Sensing*, 37, 987-999, 1999.
- 758 Ni, W., Li, X., Woodcock, C. E., Roujean, J. L., and Davis, R. E.: Transmission of solar radiation in boreal
759 conifer forests: Measurements and models, *Journal of Geophysical Research: Atmospheres* (1984–2012),
760 102, 29555-29566, 1997.
- 761 Percy, R. W., Schulze, E.-D., and Zimmermann, R.: Measurement of transpiration and leaf conductance. In:
762 *Plant physiological ecology*, Springer, 1989.

- 763 Percy, R. W. and Sims, D. A.: Photosynthetic acclimation to changing light environments: scaling from the
764 leaf to the whole plant, *Exploitation of environmental heterogeneity by plants*, 1994. 145-174, 1994.
- 765 Peng, S., Piao, S., Zeng, Z., Ciais, P., Zhou, L., Li, L. Z., Myneni, R. B., Yin, Y., and Zeng, H.: Afforestation
766 in China cools local land surface temperature, *Proceedings of the National Academy of Sciences*, 111, 2915-
767 2919, 2014.
- 768 Pisek, J., Sonnentag, O., Richardson, A. D., and Möttus, M.: Is the spherical leaf inclination angle
769 distribution a valid assumption for temperate and boreal broadleaf tree species?, *Agricultural and Forest
770 Meteorology*, 169, 186-194, 2013.
- 771 Potter, C. S., Randerson, J. T., Field, C. B., Matson, P. A., Vitousek, P. M., Mooney, H. A., and Klooster, S.
772 A.: Terrestrial ecosystem production - a process model-based on global satellite and surface data, *Global
773 Biogeochemical Cycles*, 7, 811-841, 1993.
- 774 Prince, S. D. and Goward, S. N.: Global primary production: A remote sensing approach, *Journal of
775 Biogeography*, 22, 815-835, 1995.
- 776 Pury, D. d. and Farquhar, G.: Simple scaling of photosynthesis from leaves to canopies without the errors of
777 big - leaf models, *Plant, Cell & Environment*, 20, 537-557, 1997.
- 778 Raich, J., Rastetter, E., Melillo, J., Kicklighter, D., Steudler, P., Peterson, B., Grace, A., Moore Iii, B., and
779 Vörösmarty, C.: Potential net primary productivity in South America: application of a global model,
780 *Ecological Applications*, 1991. 399-429, 1991.
- 781 Richardson, A. D., Anderson, R. S., Arain, M. A., Barr, A. G., Bohrer, G., Chen, G. S., Chen, J. M., Ciais, P.,
782 Davis, K. J., Desai, A. R., Dietze, M. C., Dragoni, D., Garrity, S. R., Gough, C. M., Grant, R., Hollinger, D.
783 Y., Margolis, H. A., McCaughey, H., Migliavacca, M., Monson, R. K., Munger, J. W., Poulter, B., Raczka,
784 B. M., Ricciuto, D. M., Sahoo, A. K., Schaefer, K., Tian, H. Q., Vargas, R., Verbeeck, H., Xiao, J. F., and
785 Xue, Y. K.: Terrestrial biosphere models need better representation of vegetation phenology: results from the
786 North American Carbon Program Site Synthesis, *Global Change Biology*, 18, 566-584, 2012.
- 787 Running, S. W., Nemani, R. R., Heinsch, F. A., Zhao, M. S., Reeves, M., and Hashimoto, H.: A continuous
788 satellite-derived measure of global terrestrial primary production, *Bioscience*, 54, 547-560, 2004.
- 789 Running, S. W., Thornton, P. E., Nemani, R., and Glassy, J. M.: Global terrestrial gross and net primary
790 productivity from the earth observing system, *Methods in Ecosystem Science*, 2000. 44-57, 2000.
- 791 Ryu, Y., Baldocchi, D. D., Kobayashi, H., Ingen, C., Li, J., Black, T. A., Beringer, J., Gorsel, E., Knohl, A.,
792 and Law, B. E.: Integration of MODIS land and atmosphere products with a coupled - process model to
793 estimate gross primary productivity and evapotranspiration from 1 km to global scales, *Global
794 Biogeochemical Cycles*, 25, GB4017, 2011.

- 795 Schaaf, C. B., Li, X., and Strahler, A.: Topographic effects on bidirectional and hemispherical reflectances
796 calculated with a geometric-optical canopy model, *IEEE Transactions on Geoscience and Remote Sensing*,
797 32, 1186-1193, 1994.
- 798 Schulze, E.-D., Kelliher, F. M., Korner, C., Lloyd, J., and Leuning, R.: Relationships among maximum
799 stomatal conductance, ecosystem surface conductance, carbon assimilation rate, and plant nitrogen nutrition:
800 a global ecology scaling exercise, *Annual Review of Ecology and Systematics*, 1994. 629-660, 1994.
- 801 Sellers, P. J.: Canopy reflectance, photosynthesis and transpiration, *International Journal of Remote Sensing*,
802 6, 1335-1372, 1985.
- 803 Sjöström, M., Zhao, M., Archibald, S., Arneth, A., Cappelaere, B., Falk, U., De Grandcourt, A., Hanan, N.,
804 Kergoat, L., and Kutsch, W.: Evaluation of MODIS gross primary productivity for Africa using eddy
805 covariance data, *Remote Sensing of Environment*, 131, 275-286, 2013.
- 806 Song, C., Katul, G., Oren, R., Band, L. E., Tague, C. L., Stoy, P. C., and McCarthy, H. R.: Energy, water,
807 and carbon fluxes in a loblolly pine stand: Results from uniform and gappy canopy models with
808 comparisons to eddy flux data, *Journal of Geophysical Research: Biogeosciences*, 114, G04021, 2009.
- 809 Strahler, A. H., Muller, J., Lucht, W., Schaaf, C., Tsang, T., Gao, F., Li, X., Lewis, P., and Barnsley, M. J.:
810 MODIS BRDF/albedo product: algorithm theoretical basis document version 5.0, MODIS documentation,
811 1999. 1999.
- 812 Verhoef, W. and Bach, H.: Coupled soil-leaf-canopy and atmosphere radiative transfer modeling to simulate
813 hyperspectral multi-angular surface reflectance and TOA radiance data, *Remote Sensing of Environment*,
814 109, 166-182, 2007.
- 815 Wang, Z., Coburn, C., Ren, X., Mazumdar, D., Myshak, S., Mullin, A., and Teillet, P.: Assessment of soil
816 surface BRDF using an imaging spectrometer, 2010, 783010-783019.
- 817 Xia, J., Chen, J., Piao, S., Ciais, P., Luo, Y., and Wan, S.: Terrestrial carbon cycle affected by non-uniform
818 climate warming, *Nature Geoscience*, 2014. 2014.
- 819 Xin, Q., Broich, M., Suyker, A. E., Yu, L., and Gong, P.: Multi-scale evaluation of light use efficiency in
820 MODIS gross primary productivity for croplands in the Midwestern United States, *Agricultural and Forest
821 Meteorology*, 201, 111-119, 2015.
- 822 Xin, Q., Gong, P., Yu, C., Yu, L., Broich, M., Suyker, A. E., and Myneni, R. B.: A Production Efficiency
823 Model-Based Method for Satellite Estimates of Corn and Soybean Yields in the Midwestern US, *Remote
824 Sensing*, 5, 5926-5943, 2013.

- 825 Xin, Q., Woodcock, C. E., Liu, J., Tan, B., Melloh, R. A., and Davis, R. E.: View angle effects on MODIS
826 snow mapping in forests, *Remote Sensing of Environment*, 118, 50-59, 2012.
- 827 Xu, L., Myneni, R., Chapin III, F., Callaghan, T., Pinzon, J., Tucker, C., Zhu, Z., Bi, J., Ciais, P., and
828 Tømmervik, H.: Diminished temperature and vegetation seasonality over northern high latitudes, *Nature*
829 *Climate Change*, 2013. 2013.
- 830 Yang, W., Ni-Meister, W., Kiang, N. Y., Moorcroft, P. R., Strahler, A. H., and Oliphant, A.: A clumped-
831 foliage canopy radiative transfer model for a Global Dynamic Terrestrial Ecosystem Model II: Comparison
832 to measurements, *Agricultural and Forest Meteorology*, 150, 895-907, 2010.
- 833 Yang, X., Strahler, A. H., Schaaf, C. B., Jupp, D. L., Yao, T., Zhao, F., Wang, Z., Culvenor, D. S., Newnham,
834 G. J., and Lovell, J. L.: Three-dimensional forest reconstruction and structural parameter retrievals using a
835 terrestrial full-waveform lidar instrument (Echidna®), *Remote sensing of environment*, 135, 36-51, 2013.
- 836 Yao, T., Yang, X., Zhao, F., Wang, Z., Zhang, Q., Jupp, D., Lovell, J., Culvenor, D., Newnham, G., and Ni-
837 Meister, W.: Measuring forest structure and biomass in New England forest stands using Echidna ground-
838 based lidar, *Remote sensing of Environment*, 115, 2965-2974, 2011.
- 839 Yi, C., Ricciuto, D., Li, R., Wolbeck, J., Xu, X., Nilsson, M., Aires, L., Albertson, J. D., Ammann, C., and
840 Arain, M. A.: Climate control of terrestrial carbon exchange across biomes and continents, *Environ. Res.*
841 *Lett.*, 5, 034007, 2010.
- 842 Yuan, H., Dickinson, R. E., Dai, Y., Shaikh, M. J., Zhou, L., Shangguan, W., and Ji, D.: A 3D Canopy
843 Radiative Transfer Model for Global Climate Modeling: Description, Validation, and Application, *Journal of*
844 *Climate*, 27, 1168-1192, 2013.
- 845 Zhang, Q., Cheng, Y., Lyapustin, A. I., Wang, Y., Xiao, X., Suyker, A., Verma, S., Tan, B., and Middleton, E.
846 M.: Estimation of crop gross primary production (GPP): I. impact of MODIS observation footprint and
847 impact of vegetation BRDF characteristics, *Agricultural and Forest Meteorology*, 191, 51-63, 2014.
- 848 Zhang, Q., Xiao, X., Braswell, B., Linder, E., Baret, F., and Moore Iii, B.: Estimating light absorption by
849 chlorophyll, leaf and canopy in a deciduous broadleaf forest using MODIS data and a radiative transfer
850 model, *Remote Sensing of Environment*, 99, 357-371, 2005.
- 851 Zhang, X., Friedl, M. A., Schaaf, C. B., Strahler, A. H., Hodges, J. C., Gao, F., Reed, B. C., and Huete, A.:
852 Monitoring vegetation phenology using MODIS, *Remote Sensing of Environment*, 84, 471-475, 2003.
- 853 Zhao, F., Yang, X., Schull, M. A., Román-Colón, M. O., Yao, T., Wang, Z., Zhang, Q., Jupp, D. L., Lovell, J.
854 L., and Culvenor, D. S.: Measuring effective leaf area index, foliage profile, and stand height in New
855 England forest stands using a full-waveform ground-based lidar, *Remote Sensing of Environment*, 115,
856 2954-2964, 2011.

857 Zhao, M., Heinsch, F. A., Nemani, R. R., and Running, S. W.: Improvements of the MODIS terrestrial gross
858 and net primary production global data set, *Remote Sensing of Environment*, 95, 164-176, 2005.
859
860